Elisabeth Kodolitsch, BSc

Porous Organic Polymers as Matrix Materials for Optical Oxygen Sensors

MASTER'S THESIS

to achieve the university degree of

Diplom-Ingenieurin

Master's degree programme: Technical Chemistry

submitted to

Graz University of Technology

Supervisor

Assoc.Prof. Dipl.-Ing. Dr.techn. Christian Slugovc

Institute for Chemistry and Technology of Materials

Graz, September 2018

EIDESSTATTLICHE ERKLÄRUNG

Ich erkläre an Eides statt, dass ich die vorliegende Arbeit selbstständig verfasst, andere als die angegebenen Quellen/Hilfsmittel nicht benutzt, und die den benutzten Quellen wörtlich und inhaltlich entnommenen Stellen als solche kenntlich gemacht habe. Das in TUGRAZonline hochgeladene Textdokument ist mit der vorliegenden Masterarbeit identisch.

Datum

Unterschrift

Danksagung

An dieser Stelle möchte ich mich bei all denjenigen bedanken, die mich während der Anfertigung dieser Masterarbeit unterstützt und motiviert haben:

Mein Dank gilt zunächst Herrn Prof. Dr. Christian Slugovc, der meine Masterarbeit betreut und begutachtet hat. Danke für die hilfreichen Anregungen und die konstruktive Kritik während den letzten sechs Monaten.

Ebenfalls möchte ich mich bei Petra Kaschnitz und Josefine Hobisch bedanken, für die zahlreichen Messungen und Auswertungen die sie im Laufe meiner Arbeit durchgeführt haben. Ein weiterer Dank geht an PyroScience, für die optischen Sauerstoffsensoren, die im Zuge dieser Arbeit für die Messungen verwendet wurden.

Ein besonderer Dank gilt auch der gesamten Arbeitsgruppe, insbesondere Petra Hofstadler und Christian Leypold, die mir mit zahlreichen Hilfestellungen und Ideen bei jeglichen Problemen zur Seite standen. Danke für die angenehme Atmosphäre (und Schokolade) während meiner gesamten Zeit am Institut.

Meinen Freunden Anita, Yvonne und meiner Schwester Katharina danke ich besonders für den starken emotionalen Rückhalt, die Hilfe und die schöne Zeit über die Dauer meines gesamten Studiums. Danke auch an meinen Freund Michael, der immer hinter mir gestanden und mich unterstützt hat.

Abschließend möchte ich mich bei meinen Eltern bedanken, für jegliche Unterstützung in meinem Leben. Danke, dass ihr mir das Alles ermöglicht habt ohne euch wäre ich nicht so weit gekommen.

Abstract

In this work three potentially microporous polymers were prepared, characterized and tested as matrix materials for optical oxygen sensing. The first polymer is based on the monomer 5,12-dimethoxy-1,4-dihydro-1,4-methanotetracene which was oligomerized via a Diels-Alder reaction and the such obtained macro monomer was subsequently polymerized through Ring-opening Metathesis Polymerization (ROMP). The second polymer was prepared through ROMP of exo-1,4,4a,9,9a,10-hexahydro-9,5(1‘,2‘)-benzeno-1,4-methanoanthracene (HBM) which is accessible through a Diels-Alder reaction of anthracene with 2,5-norbornadiene. The third polymer resulted from hydrogenation of the second one. All synthesized polymers were characterized via gel permeation chromatography, nitrogen absorption measurements and differential scanning calorimetry. All three polymers exhibited good film forming properties, which allowed for the assessment of their qualification as matrix material in optical oxygen sensors. The oxygen permeability increased in the order hydrogenated HBM < poly(styrene) (used as a reference) < HBM < first polymer.

Kurzfassung

In dieser Arbeit wurden drei potenzielle mikroporöse Polymere hergestellt, charakterisiert und als Matrixmaterialien für die optische Sauerstoffmessung getestet. Das erste Polymer basierte auf dem Monomer 5,12-Dimethoxy-1,4-dihydro-1,4-methanotetracen, das über eine Diels-Alder-Reaktion oligomerisiert wurde. Das so erhaltene Makromonomer wurde anschließend durch eine ringöffnende Metathese Polymerisation (ROMP) polymerisiert. Das zweite Polymer wurde durch ROMP von exo-1,4,4a,9,9a,10-Hexahydro-9,5(1',2')-benzo-1,4-methanoanthracen (HBM) hergestellt, welches durch eine Diels-Alder-Reaktion von Anthracen mit 2,5-Norbornadien gewonnen wurde. Das dritte Polymer resultierte aus der Hydrierung des zweiten.

Alle synthetisierten Polymere wurden durch Gel-Permeations-Chromatographie, Stickstoffabsorptionsmessungen und Differentialthermoanalyse (DSC) charakterisiert. Des Weiteren zeigten alle drei Polymere gute filmbildende Eigenschaften, die es ermöglichten, ihre Eignung als Matrixmaterial in optischen Sauerstoffsensoren zu untersuchen. Die Sauerstoffpermeabilität stieg in der Reihenfolge hydriertes HBM < Polystyrol (als Referenz verwendet) < HBM < erstes Polymer an.

Table of Content

1. Introduction

Natural gas, which consists mostly of methane is generally available in large quantities and environmentally preferred over other hydrocarbon fuels, due to its cleaner combustion. For the usage of methane in a large-scale, a safe and economical way for its storage has to be developed.[3] Therefore, the storage of natural gas in highly porous materials has been proposed as an innovative way. Many materials have been investigated including carbons, zeolites and metal organic frameworks (MOFs), but in some cases there are limitations regarding the thermal and chemical stability. MOFs, for example, are sensitive in the long term to polar substances such as water, that could degrade the material during its lifetime. Due to that reason, porous organic polymers (POPs) offer a valid option. POPs are a type of highly cross-linked polymers which are mainly characterized by their amorphous structure and their possession of micro pores.[4] Due to the connectivity of the carbon-carbon bonds, they impart high thermal and chemical stability and a high resistance to contaminants. In a series of studies in the field of POPs, polymers with a very high specific surface area could be synthesized, rivaling those for MOFs. Such materials were characterized using several techniques, including thermal analysis and nitrogen adsorption measurements in order to gather information about their thermal stability and their gas storage capacity.[5]

2. General Aspect

2.1 Porous polymeric materials

Porosity can be generally viewed as profound concept to understand nature and how it creates advanced structures. By having a closer look into the nature there can be found a great variety of different structures associated with certain porosity. Some interesting examples are hollow bamboo, alveoli in lungs and honeycomb with hexagonal cells. The design and construction of porous architectures that mimic those structures has gained significant attention in recent times. The developing field of porous polymers down to the micro- and nanoscale range has received an increased level of interest, because of their potential to merge the properties of both polymers and porous materials. They can be designed to combine advantages like a well-defined porosity and high surface areas with mechanical properties typical for polymers.[6,7,8,9] Thereby, the surface area, pore geometry and pore size are the most important aspects of porous polymers on which depends their applicability. In principle, the surface area of such a network is governed by pore surface and pore size. The introduction of functional moieties and the molecular dimension of the monomeric units are able to tune the physical structure of the pores and the pore surface functionalities. The obtained constitution of the framework depends thereby on the type of reaction, the reaction conditions and the monomers employed.[9,10,11,12]
On account of this huge variety of modification and functionalization of the framework, porous polymers can be used in various applications, for example, in gas adsorption and storage, gas separation and selective permeation, adsorption of organic pollutants, as photoconductors, in catalysis and in clean energy storage.[9,12]

Generally, porous materials can be divided into three groups: purely inorganic materials, purely organic materials and organic-inorganic-hybrid materials as shown in Figure 1. Porous inorganic materials cover a range of solids and can either be crystalline or amorphous. For example, zeolite and silica molecular sieves are classified as such materials. Highly stable, cheap and abundant building blocks make them favourable in industrial

applications, especially in those requiring high temperatures. However, inorganic porous materials suffer from a lack of functionalities in a wide application range.

Crystalline materials such as metal organic frameworks (MOFs) mimic the ordered micropore-structure of zeolites. They can be classified as organic-inorganic hybrid material.[4,13,14] They exhibit exceptional surface areas and the introduction of functionalities is rather easy. Unfortunately, the instability and sensitivity of coordination bonding in an ambient atmosphere is limiting the extraordinary properties of MOFs to be applied broadly.[15]

Porous materials refer to hydrocarbons are called purely organic and can be separated into amorphous or crystalline structures. Considering that, covalent-organic frameworks (COFs) exhibit crystalline structures and porous organic polymers (POPs) amorphous structures.[4] Crystalline networks have uniform pore size, whereas amorphous networks exhibit a wider pore size range. The network of crystalline porous polymers is thereby formed by using reversible bond chemistry.[12]

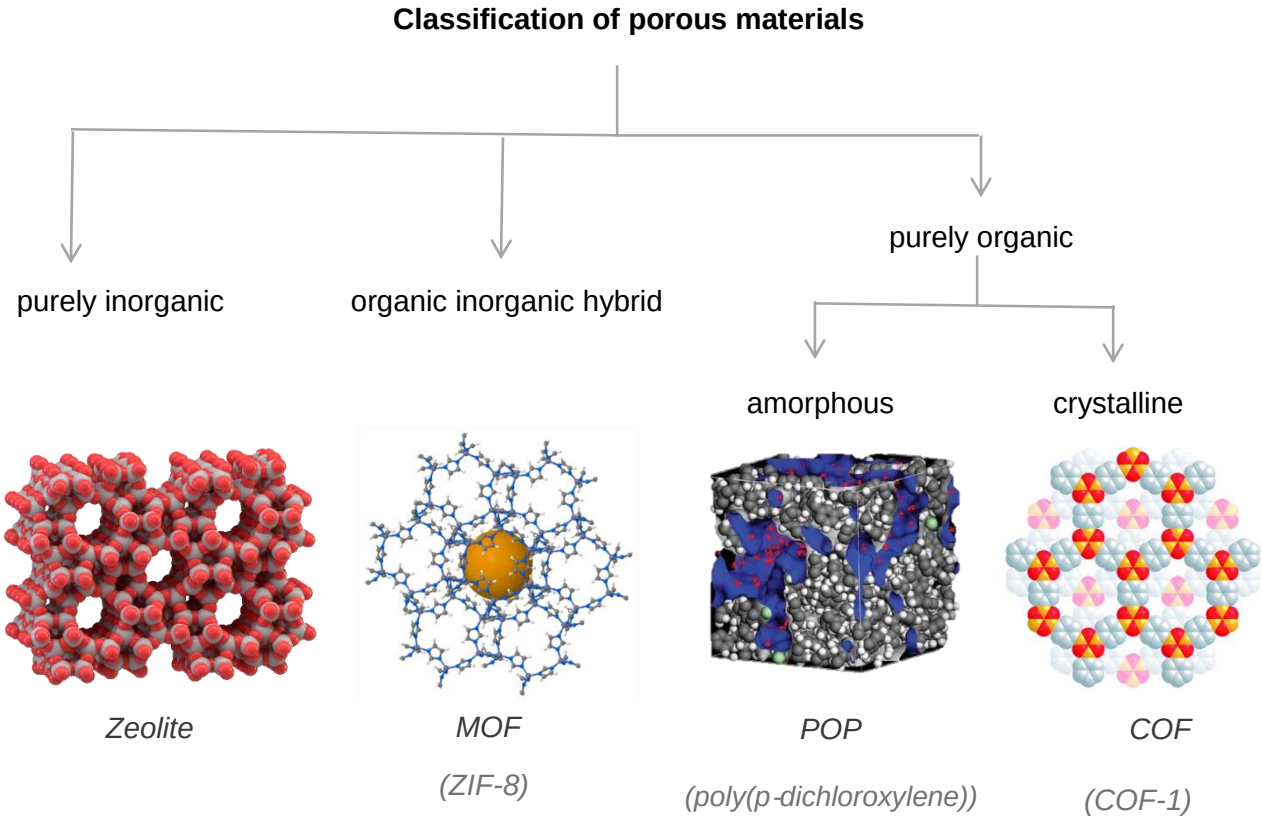

Figure 1: Classification of porous materials

2.1.1 Microporous polymers

By encouraging the use of Internal Union of Pure and Applied Chemistry nomenclature (IUPAC)[16] we define microporous polymers as polymeric material with pore size smaller than 2 nm in diameter. Mesoporous polymers are generally defined with pore size in the range of 2-50 nm and macroporous polymers with pore size larger than 50 nm.[9,14]
The synthesis of microporous polymers means a great challenge, due to much higher capillary pressures and surface energies compared with meso- and macroporous counterparts. There are several important structural characteristics describing microporous polymers including pore geometry, pore surface functionality, pore size and polymeric framework structure. The framework structure can be further described by their topology, functionality and their composition as shown in Figure 2.[17,18] The pore geometry includes tubular, network-type and spherical morphologies that can be assembled into ordered or disordered arrays.[9]

The surface area is a very important parameter that is used to evaluate the pore structure. In general, pores with a smaller size contribute to the generation of materials with higher surface areas. The pore surface and framework functionalities can be designed by the use of functional monomers or by postmodification processes.[9] Pre-designed framework modification and the insertion of functionalities can be utilized to serve two purposes: firstly, to impose new functions onto these polymers and secondly, to improve existing properties. Pore dimension and surface area can thereby be modified in a quantized fashion by the control of the strut length and the pore size can be inversely variated with the side-chain length.[12] This strongly limits the selection of the monomers to be used and their linking chemistry. Requirements on monomers which provide a very robust framework structure, whether planar or contorted and sufficient mechanical stability are of highest priority.

Further modification of changing monomer structure and reactivity is accomplished by changing the reaction conditions including solvent, catalysts, temperature, concentration of the reactants and their ratios. This aspect is also important to maximize the cost-performance ratio of the microporous polymer.

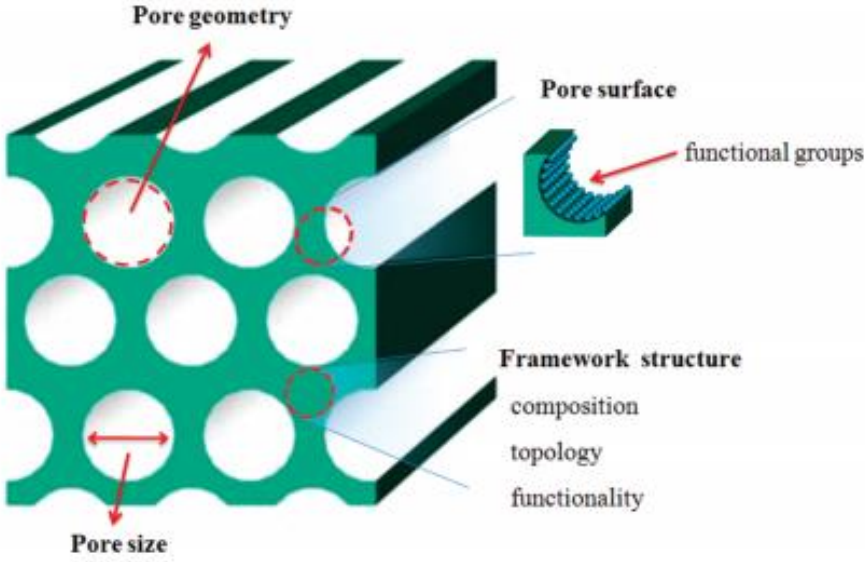

Figure 2: Illustration of pore geometry, pore surface, pore size and framework structure of porous polymers[9]

2.1.1.1 Metal organic frameworks - MOFs

Metal organic frameworks are in general porous coordination polymers that are highly crystalline and contain metal-organic hybrids.[19,20] They can be produced from multidentate organic ligands (e.g., sulfonates, tetrazolates and carboxylates) and metal-containing clusters (secondary building blocks) through the formation of coordination bonds.[19,21] The combination of those two components provides endless possibilities. This flexibility with which the constituent's geometry, functionality and size can be varied has led to over 20,000 different MOFs being reported. A very well studied MOF is shown in Figure 3.[22]

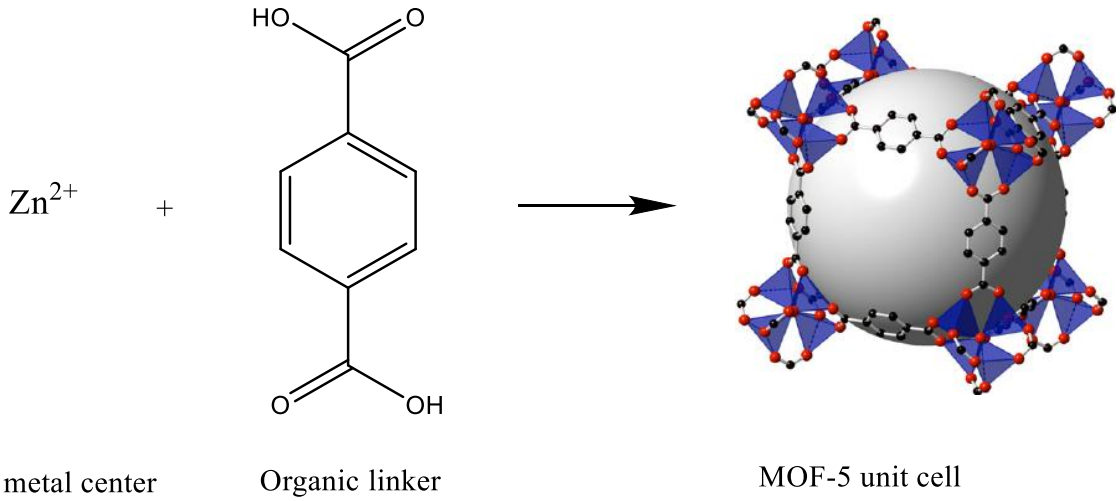

Figure 3: Synthesis of MOF-5 from a Zn metal cluster and terephtalic acid[23]

MOFs are characterized by typical porosities greater than 50 % of the crystal volume and surface areas in the range of 1,000 to 10,000 m^2/g, exceeding those of materials such as zeolites and carbons.[22] They exhibit tuneable pore size and adjustable internal surface properties. These properties make MOFs of great interest for potential applications in gas storage and separation, catalysis and ion transport. Additional applications in fuel cells, catalytic conversions, and supercapacitors increasingly gaining importance in industrial-scale production.[20]

2.1.1.2 Covalent organic frameworks - COFs

COFs are crystalline microporous materials which are synthesized from organic molecules, linked by strong covalent bonds.[24] Light elements like hydrogen, boron, carbon, nitrogen, and oxygen, which make up the COFs are known to generate these strong covalent bonds.[25]

They build up a network of two- and three-dimensional organic structures with a robust architecture, high porosity, a high chemical and thermal stability and low densities. The specific surface area of the COFs is surpassing those of zeolites and porous silicates.[26]

These periodic frameworks are formed of secondary building units through various combinations. Thereby, COF materials exhibit superior potential in diverse applications such as gas storage, separation and heterogeneous catalysis.

In order to construct the polymeric structure of COF materials with both structural regularity and porosity, many limitations still exist. The structural regularity of these materials is much difficult to control via the strong covalent bonds, in contrast to MOF systems, where the assembly of building units could well be self-adjusted via the coordination bonds. Due to a large variety of synthesis routes, the reaction shown in Figure 4 is based on the reversible formation of boronate anhydride from dehydration of boronic acid. Via this reaction the first COF material, COF-1 was synthesized.[24, 26]

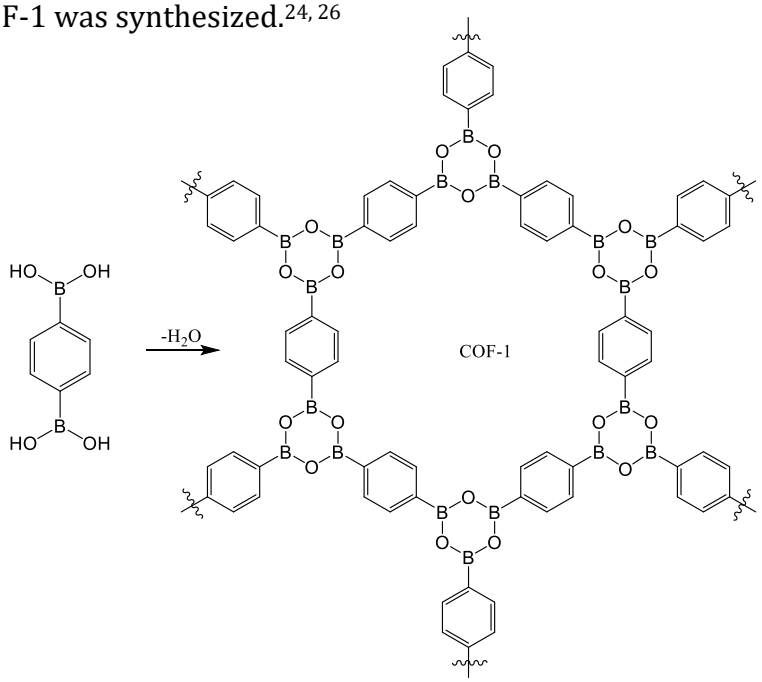

Figure 4: Boron condensation to COF-1[26]

The COF-1 polymer (Figure 4) is characterized by a high thermal stability of temperatures up to 600 °C, a high surface area of around 711 m^2/g and permanent porosity.[27]

2.1.1.3 Porous organic polymers - POPs

POPs are a type of highly cross-linked polymers which are mainly characterized by their amorphous structure and their possession of micro pores. Their porosity is related to materials like metal organic frameworks and zeolites. POPs arguably the easiest to synthesize among the three classes of porous materials, because they are noncrystalline and have nonuniform pores, that are typically somewhat ill-defined. Thereby, their behavior is more difficult to understand and their design more difficult to control.

Porous polymers can be generally synthesized by incorporating di- or multitopic monomers with three or more connection points, into well-known chain-growth and step-growth polymerization processes. These processes can rather proceed radical, anionic, cationic or by a condensation reaction. Subsequently, they provide cross-links between the propagating polymer chains and led to the formation of a three-dimensional (3D) network. As typical in many porous materials, POPs can only achieve permanent microporosity by the use of comparatively rigid monomers. When they are cross-linked, there can be obtained pores with similarly rigid walls. In contrast to macroporous polymeric materials, where the degree of cross-linking depends on the concentration of the added cross-linking molecules, the cross-linking in POPs depends only on the monomeric units. Accordingly, the monomers have to possess higher valency/topicity and more complex shapes. As mentioned before, POP pore size can be difficult to control synthetically, if cross-links form quickly and irreversibly or if framework interpenetration occurs.[4]

In a series of studies in the field of POPs, polymers with a very high specific surface area could be synthesized, rivaling those for MOFs. For example, POPs prepared by linking tetrakis(phenyl) subunits have been obtained with specific surface areas of around 5,640 m^2/g.[28]

A disadvantage of the amorphous nature of POPs is the perspective of structural characterization. On the other hand, viable materials can be obtained rapidly with no need to wait for crystal formation.[4]
In general, due to their high gas uptake capacity and their easy functionalization, they access ideal properties for methane capture. POPs are widely found in applications in the field of gas adsorption and separation, optoelectronic devices, chemo sensors and catalysis.[9,1,15]

In the course of this work one-dimensional (1D) linear polymers with a high level of cross-linking and flexible backbones have been prepared through ring opening metathesis polymerization. One-dimensional linear polymers usually have low surface areas due to the flexible nature of the polymer which led to dense-packing in the solid state. To achieve non-cross-linked porous organic polymers, structurally rigid building blocks and ladder-typed backbones have been used. In literature, those polymers were found to exhibit also high surface areas in comparison to the three-dimensional networks.[1]

2.1.1.3.1 POPs prepared via Ring Opening Metathesis Polymerization

The Ring Opening Metathesis Polymerization, also called ROMP, is among the most efficient controlled living polymerization method. To achieve a porous ROMP polymer noncompliant and rigid moieties are densely incorporated into the polymer backbone to prevent the folding of the polymer to the collapsed state, as already mentioned before.[1]

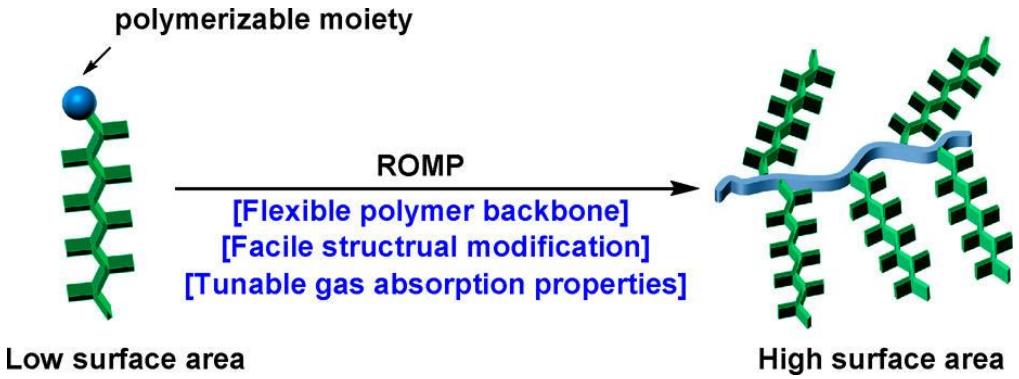

Figure 5: POPs synthesized through ROMP[1]

In general ROMP is a chain growth polymerization process where cyclic olefins are converted to polymeric material. The mechanism is based on olefin metathesis, which is a unique carbon-carbon double bond exchange process mediated by a metal.[29] Any unsaturation associated with the monomer can be conserved as it is, converted to the polymer.

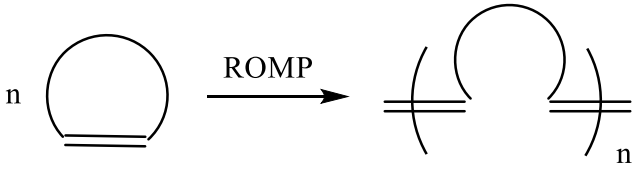

Figure 6: General example of a ROMP reaction

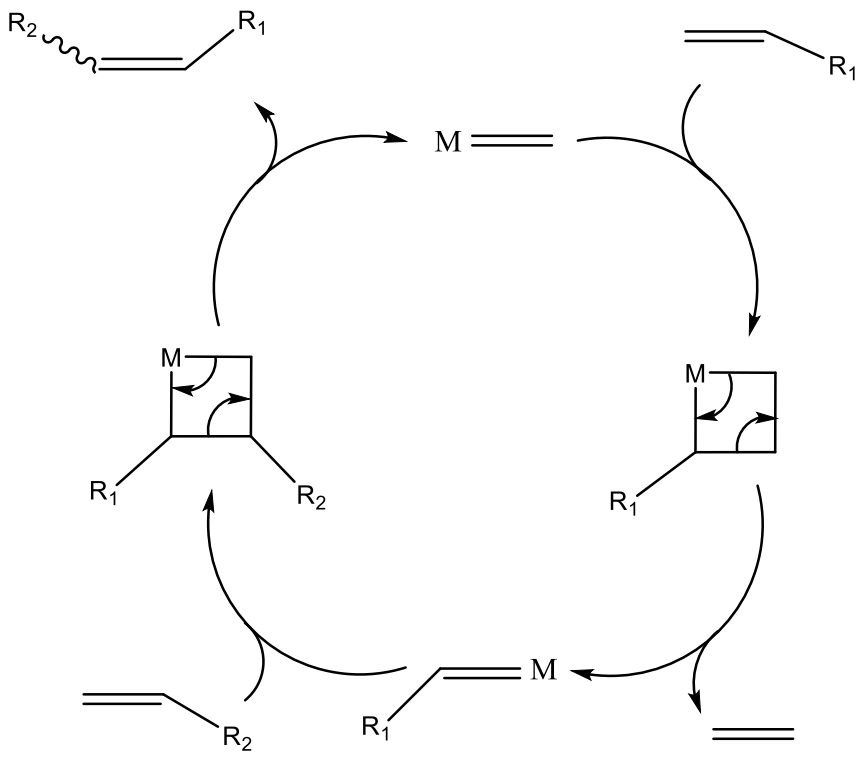

Figure 7: Chauvin mechanism

The mechanism of the ROMP is based on Chauvin's original proposal, shown in Figure 7.[30]
A transition metal alkylidene complex coordinates to a cyclic olefin to start the initiation. Subsequently a four-membered metallacyclobutane intermediate is generated by a [2+2]-cycloaddition. A cycloreversion reaction is associated to afford a new metal alkylidene, which has increased in size and has a reactivity toward cyclic olefins similar to the initiator.
Analogous steps are repeated until the polymerization ceases for reasons like a reaction equilibrium is reached, all monomers are consumed or the reaction is terminated. This reaction step is called propagation stage. The reaction is usually quenched through the addition of specialized reagents, like ethyl vinyl ether for Ru mediated polymerizations. The function of this reagent is the detachment of the metal from the end of the polymer chain by installing a new functional group instead. The ethyl vinyl ether provides a methylidene end- functionalized polymer and a [Ru]=CHOEt type complex.[31]

2.1.1.3.2 Initiators

2.1.1.3.2.1 Ruthenium

The first well-defined single-component ruthenium complex showing activity in ROMP was $(PPh_3)_2Cl_2Ru=CH-CH=CPh_2$.[32] The complex generally exhibit indefinitely stability in the solid state and no decomposition after exposure to water, ethers, or various alcohols. At first attempts, the Ru catalyst did not show appreciable activity toward olefins excepted of cyclobutene and norbornene derivates, and accordingly the attention shifted toward optimizing the ligand environment of the ruthenium center. The optimization of the activity was managed by varying the nature of the phosphine ligand. The use of electron rich and bulky phosphines, for example PCy_3, was found to be very effective. The resulting complex $(PPCy_3)_2Cl_2Ru=CH-CH=CPh_2$ was more stable toward organic acids, strong inorganic acids and achieved a broader range of tolerance toward functionality.[31]

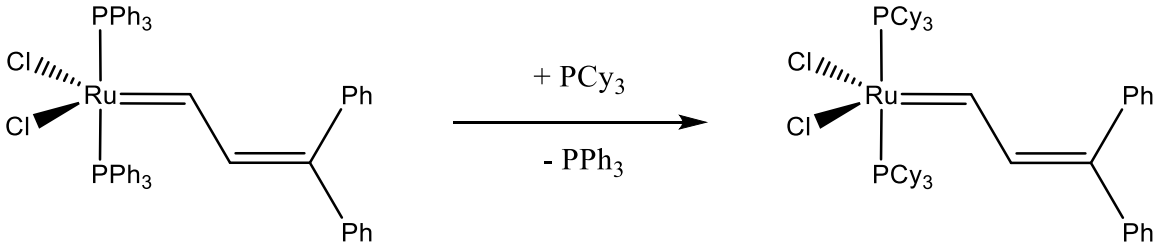

Figure 8: Modification of the Ru catalyst

The catalyst shown in Figure 8 is also called “first-generation” type, because of its two phosphine ligands. The second-generation catalyst has the same use in organic chemistry, but is even more stable and more active than their predecessors. In contrast to a first-generation catalyst, they are substituted with one phosphine ligand and one electron-donating N-heterocyclic carbene (NHC). It generally requires a lower catalyst loading, but because of its faster propagation than its initiation, they can give a broad polydispersity.[33,34] Shown in Figure 9 a mesityl group is used as NHC-substituent.

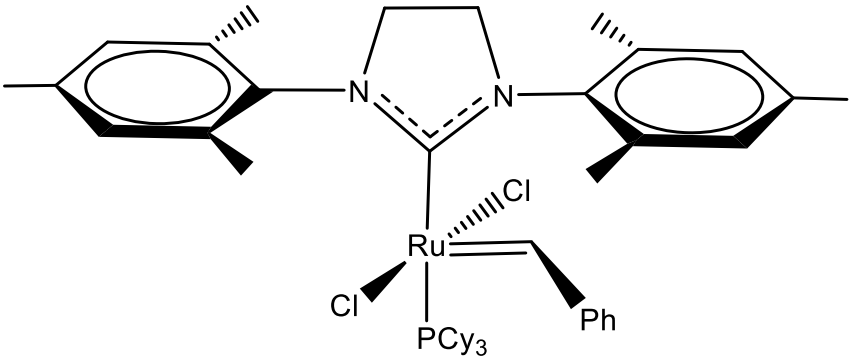

Figure 9: 2nd generation Grubbs catalyst

The modification of the 2nd generation catalyst by replacing the phosphine ligand with more labile pyridine ligands, leads to the establishment of the 3rd generation Grubbs catalyst. They are used in ROMP because of their fast initiation rate. The ratio of the rate of initiation to the rate of propagation is very high, making them useful in living polymerization and yielding in a low polydispersity.[35]

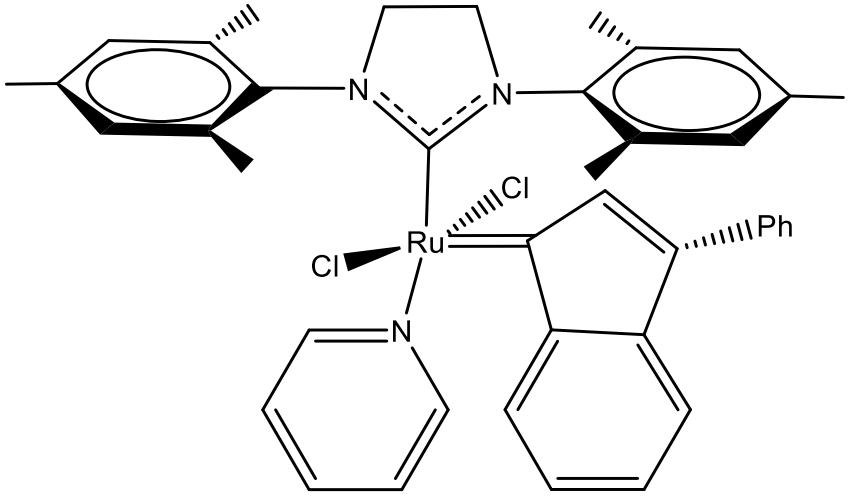

Figure 10: 3rd generation Grubbs catalyst (M31)

2.1.1.4 Cyclic olefin copolymers - COCs

In the course of this work, a second polymer was synthetized, classified as subcategory of porous organic polymers (POPs).

COPs are a class of amorphous polymers based on different types of cyclic monomers and polymerization methods. They can be produced by chain (co-)polymerizations e.g., by ring-opening metathesis polymerization followed by hydrogenation of the cyclic monomers.[36] The polymerization of only one single type of monomer leads to the cyclic olefin polymers, also called COPs. COCs and COPs are very attractive thermoplastic resins with unique advantages like high transparency, high heat stability, good chemical resistance and a low density. Varying the comonomer employed and content it is possible to control and modify the properties of the COCs. For the use in some applications a high glass transition temperature (T_g) is a requirement for a good dimensional stability under high temperature. This can be achieved by increasing the cycloolefin content in the polymer chain, or employing a bulkier cycloolefin monomer. Due to the steric effect, the T_g can be improved at relatively low comonomer incorporations.[37] A COC with a high T_g of around 201 °C is shown in Figure 11.[38] The figured ethylene/norbornene (NB) copolymer is the representative COC. They are mostly used for packaging films or in optical films, like lenses, mobile devices, displays and touchscreens.[33]

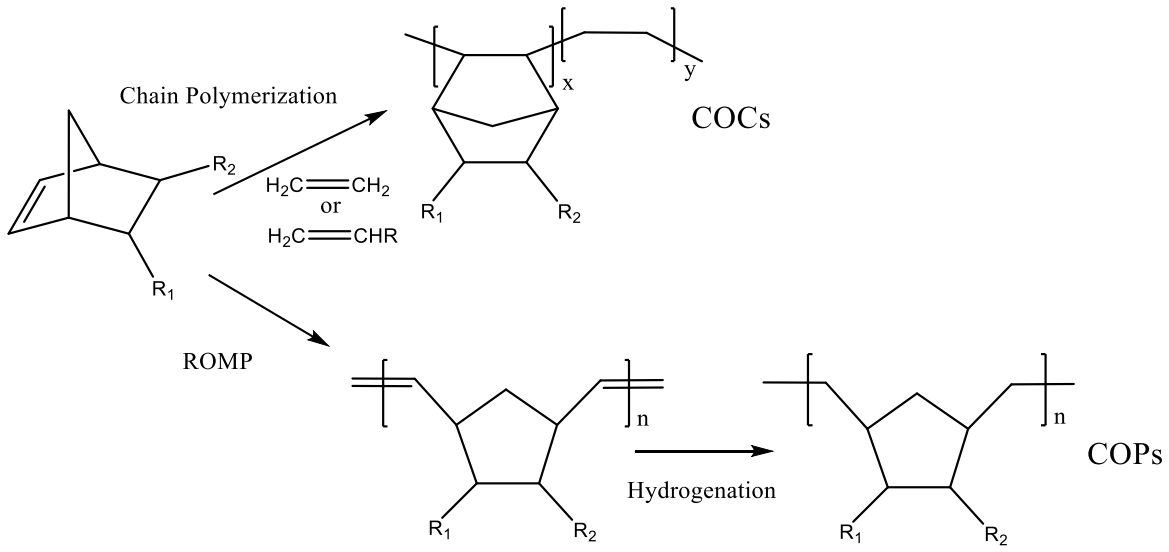

Figure 11: Polymerization routes for COCs and COPs[33]

2.1.1.5 PolyHIPEs

Furthermore, a PolyHIPE was prepared, with the aim to synthesize another microporous material. Emulsions in which the volume of the dispersed ("internal") phase occupies more than 74 % of the total volume, are called HIPEs. Water is used as dispersed aqueous phase containing a water-soluble initiator. The continuous phase, which can contain monomers and crosslinking monomer make up less than 26 % of the total volume. In addition, an organic soluble, hydrophobic surfactant is required to form the organic phase.[39,40] The polymerization of the continuous phase of an HIPE, leads to the polymerized high internal phase emulsion, also called polyHIPE.

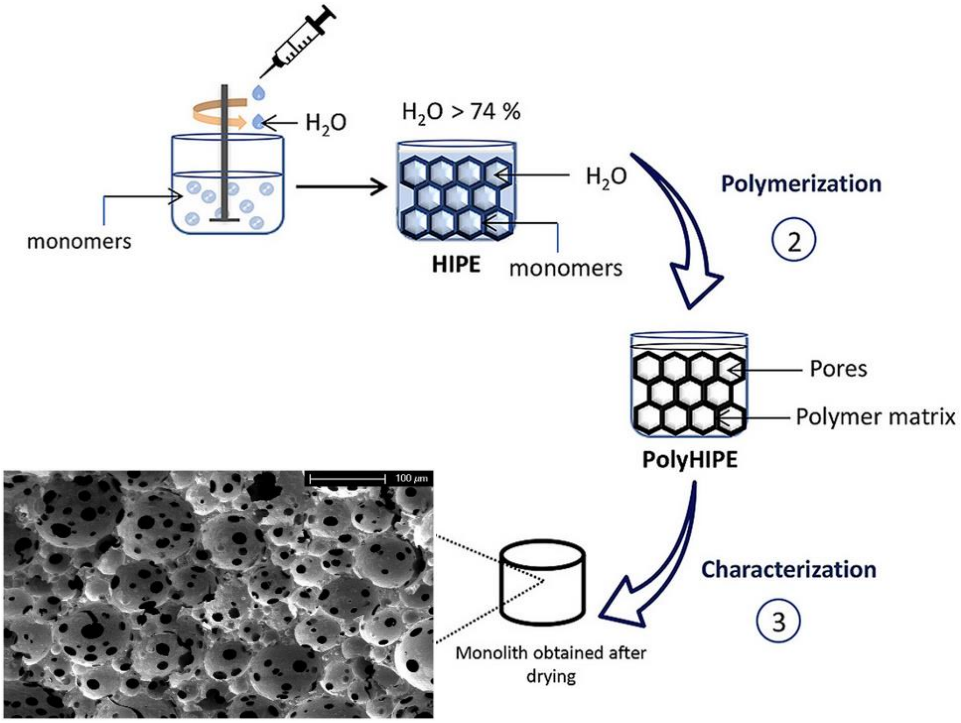

Figure 12: Preparation and structure of a PolyHIPE[41,42]

This obtained porous polymer monoliths are of high interest, because of their open interconnected pore network structure. These structure (Figure 12) consists of spherical cavities, which are referred as "voids". Voids are connected by pores, which are also called "windows".[40] PolyHIPEs can be used in several applications like separation membranes, tissue engineering scaffolds or templates for porous ceramics.

3. Results and Discussion

The aim of this thesis was to synthesize two different monomers, Monomer 1 (**3**) and Monomer 2 (**5**). After the oligomerization reaction of compound **3**, polymerization of the oligomer (**4a**) via ROMP was attempted.

Compound **5** was polymerized via ROMP without a previous oligomerization reaction to polymer **5a**. Afterwards, it was attempted to hydrogenize **5a** to compound **6**, in order to alter the chemical properties and improve the thermal and oxidative stability.

4a and the respective polymer (**4b**) of compound **3** and the respective polymer of compound **5** and **6** that were synthesized, were characterized via GPC, nitrogen absorption measurements and DSC analysis.

Furthermore, the synthesised polymers (**4b**), (**5a**) and the hydrogenized polymer (**6**) were characterized by a quenched- phosphorescence oxygen sensing to measure the oxygen permeability of the matrices.

3.1 Monomer synthesis and characterization

Within the scope of this Master's thesis, two target monomers (**3** and **5**) were successfully isolated. An overview of these prepared compounds is given in Figure 13 and Figure 14.

First of all, in order to synthesize compound **3**, a reduction using sodium borohydride leading to compound **1** was performed. In the next step, the formation of 1,4,4a,12a-tetrahydro-1,4-methanonaphthacene-5,12-dione (**2**) was realized by a Diels-Alder-reaction of compound **1** using cyclopentadiene as a reagent. Afterwards, reduction by sodium hydride and subsequent alkylation reaction with methyl iodide led to the formation of the desired product 5,12-dimethoxy-1,4-dihydro-1,4-methanotetracene (**3**).

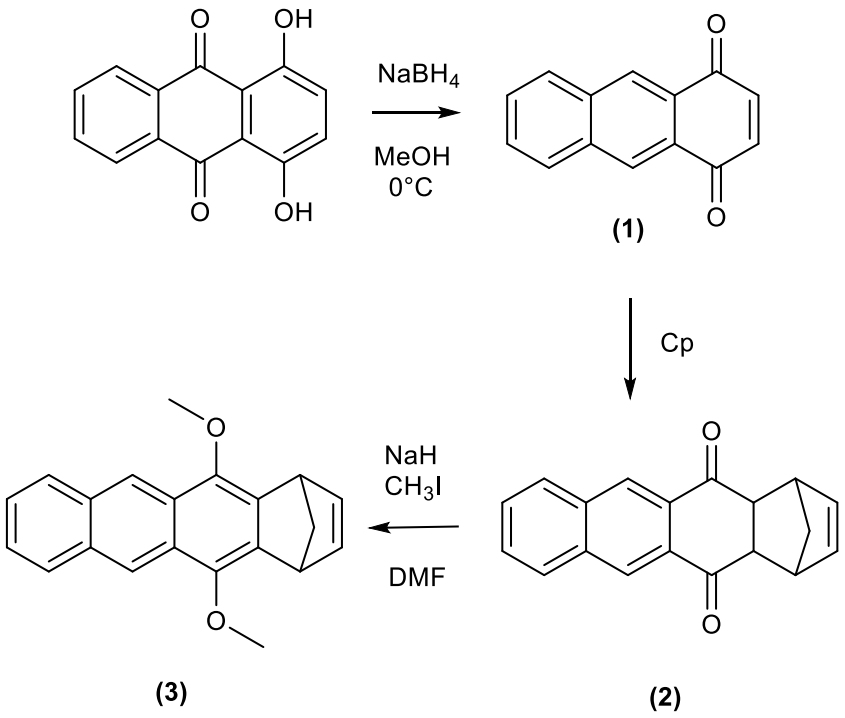

Figure 13: Synthetic scheme of compound **3**

The second monomer (**5**), exo-1,4,4a,9,9a,10-hexahydro-9,5(1‘,2‘)-benzeno-1,4-methanoanthracene (HBM), was prepared through a Diels-Alder reaction of anthracene with 2,5-norbornadiene.

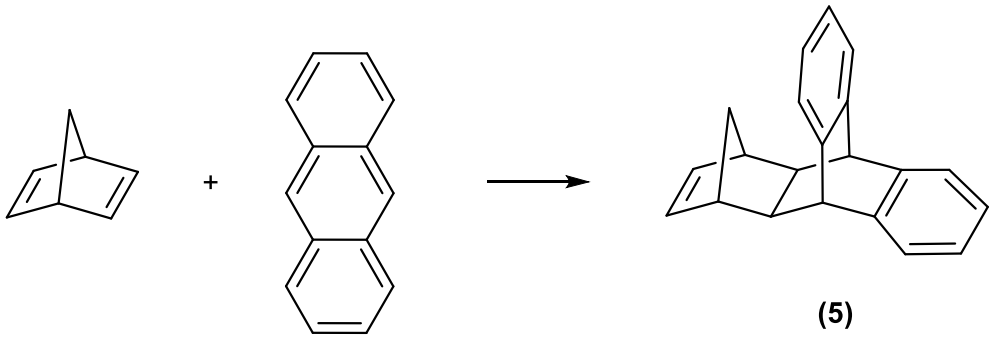

Figure 14: Synthetic scheme for **5**

In the following section, the synthesis of monomer 1 and monomer 2 and respective analysis data will be discussed.

3.1.1 Synthesis of monomer 1 (**3**)

In this section the synthetic steps and encountered difficulties during the preparation of monomer 1 will be discussed.

3.1.1.1 Reduction using $NaBH_4$

In order to synthesize compound **1**, quinizarine was used as a starting material. This crystalline compound, which is known under the name 1,4-dihydroxyanthraquinone, exhibits an intense orange color. Formally, it is derived from anthraquinone by replacing two hydrogen atoms with hydroxyl groups. The applications of quinizarine cover a wide range; amongst others it can act as a coloring agent for gasoline and heating oils and might also be used as a pH-indicator.[43] While the protonated structure of this compound exhibits an orange color, deprotonation leads to a purple appearance, wherefore it is excellently suitable for the application as a pH indicator.[44]

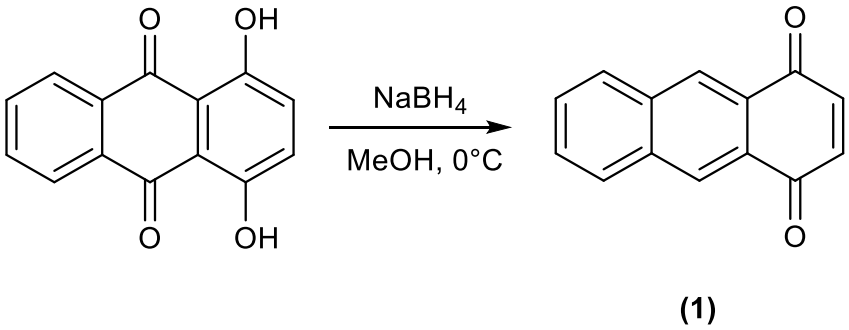

Figure 15: Reduction of quinizarine

Regarding the synthesis of compound **1**, which was aimed during this thesis, quinizarine was subjected to a reduction step using sodium borohydride, in order to yield 1,4-anthraquinone (**1**). The reaction was carried out under inert atmosphere of nitrogen. Furthermore, cooling of the reaction mixture to 0 °C was required, due to the exothermic character of the reduction reaction using sodium borohydride. After addition of $NaBH_4$ the release of formed hydrogen gas could be observed.

The primarily intense orange color of the reaction mixture changed to a brownish color after a reaction time of one hour, indicating conversion of the quinizarine educt.

After quenching the reaction mixture with 6 M HCl, a cloudy mixture containing an orange-brown colored precipitate was observed. Further work-up included a washing step with deionised water and filtration of the mixture. The solvent was evaporated under reduced pressure, yielding the crude product as an orange-brownish solid.

According to literature,[45] using only 1 eq. of $NaBH_4$ for this type of reaction, might led to the formation of unwanted sided products; one of these compounds that can typically occur is shown in Figure 16.

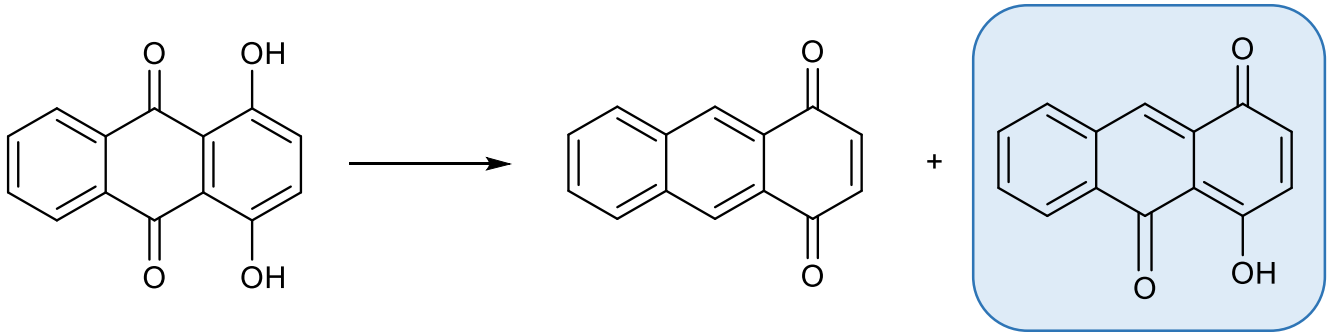

Figure 16: Formation of 4-hydroxyanthracene-1,10-dione

Although the formation of side-products is stated in literature, the formation of such compounds could not be observed according to performed TLCs. However, it was shown that no full conversion of the educt could be obtained, even after 19 hours' reaction time. The TLC (CH:EE 10+1) of the reaction mixture is shown in Figure 17. The unreacted quinizarine has an R_f value of 0.41 while the product shows a value of 0.24.

R_f = 0.41

R_f = 0.24

Figure 17: Reaction conversion after 19 h

By changing the reaction conditions and adding 4 eq. of the reducing agent $NaBH_4$, still no full conversion could be detected via TLC. Therefore, it was decided to investigate the reaction progress after addition of 6 eq. The alteration of the reaction conditions and the respectively obtained yields after purification are shown in Table 1.

Table 1: Variation of the reducing agent

$NaBH_4$ (eq.)	**Reaction time (h)**	**Product (% yield)**
1	19	no work up
4.9	24	79.9
6.63	24	73

The amount of conversion of the educt to the desired compound **1** was determined via ^{1}H- NMR spectroscopy.

In Figure 19 the 1H-NMR spectrum of the educt quinizarine is shown. Compared to the spectrum of the reaction mixture (Figure 18) it can be observed that quinizarine was still present and no full conversion to the desired product could be observed.

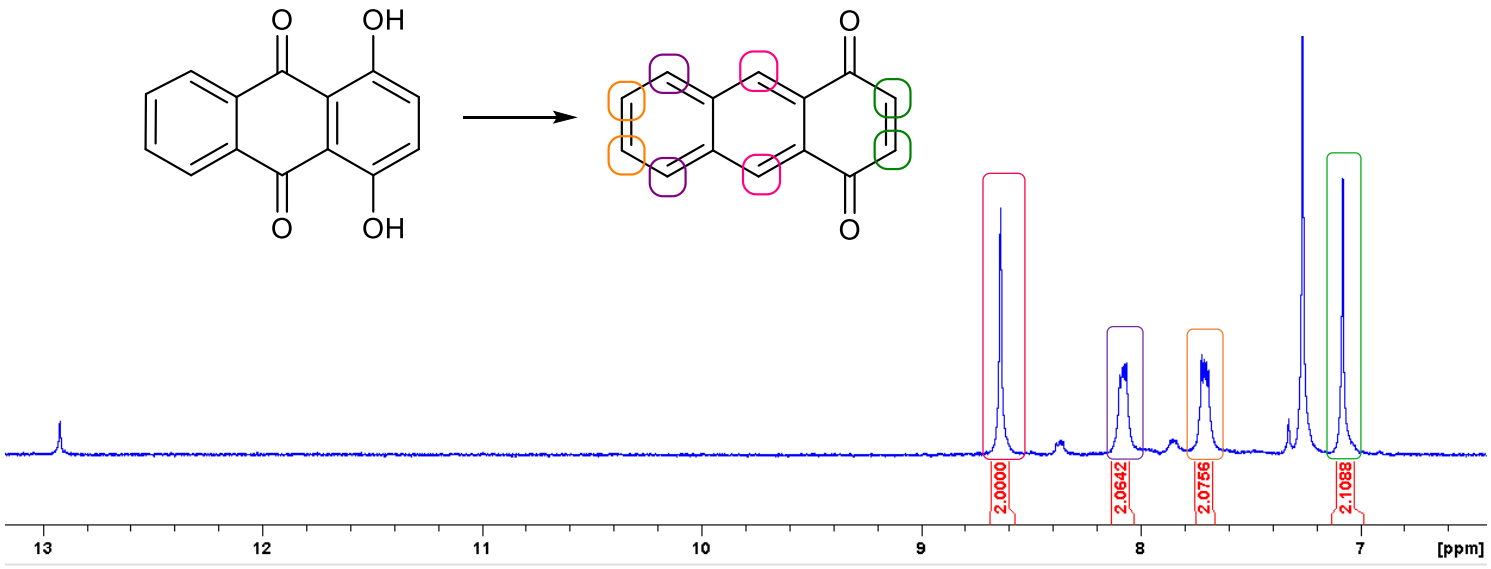

Figure 18: ^{1}H-NMR peaks related to 1,4-anthraquinone

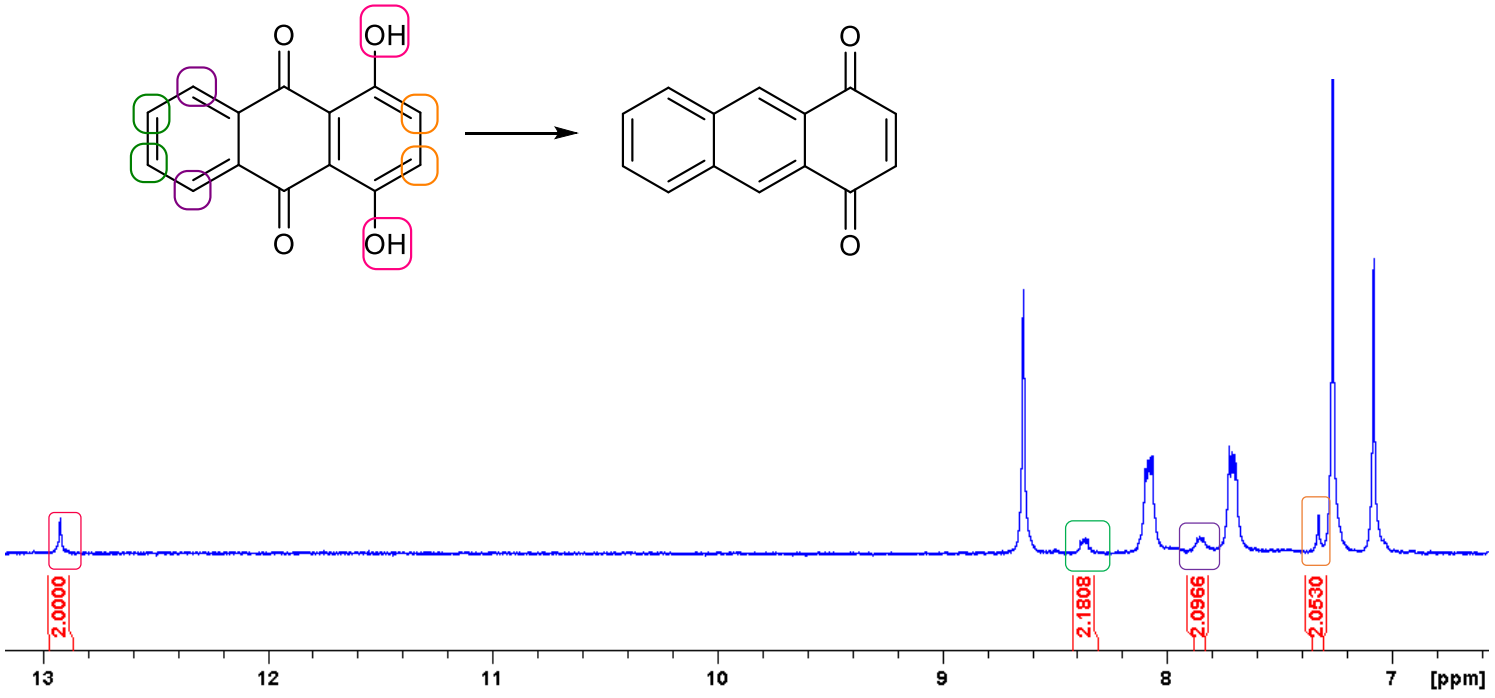

Figure 19: ^{1}H-NMR peaks related to quinizarine

In order to purify the obtained product from traces of educt, a column chromatography was performed (CH:EE 3+1). Due to the reason that the movement of quinizarine was bad on TLC plates and the silica column and the elution times of educt and product were similar, it was a challenging task to separate the product from the unreacted educt and to obtain it in pure yield.

According to ^{1}H-NMR spectroscopy, traces of quinizarine were still present even after purification via column chromatography. It might be useful to consider other purification methods for the future performance of this synthesis.

3.1.1.2 Diels-Alder-cycloaddition

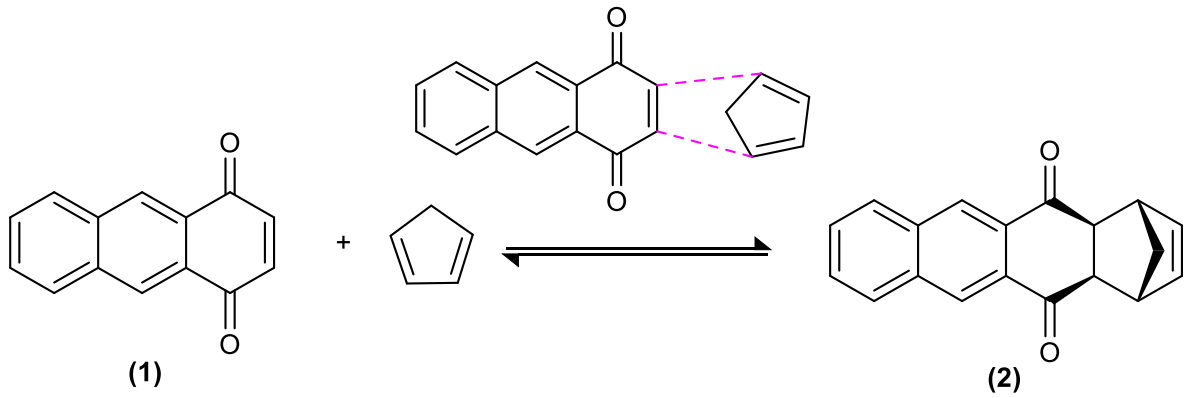

Figure 20: Diels-Alder-cycloaddition

The second step of the monomer 1 synthesis included the conversion of 1,4-anthraquinone (**1**) to 1,4,4a,12a-tetrahydro-1,4-methanonaphthacene-5,12-dione (**2**) by a Diels-Alder-reaction. This so called [4+2] cycloaddition takes place between a conjugated diene and an electron deficient olefin (dienophile). During this reaction, electrons are transferred in a cyclic fashion between the dienophile and the diene, in order to form a cyclic structure. One example of this type of reaction is shown in Figure 20, whereby compound **1** acts as the dienophile, while the cyclopentadiene reagent plays the role of the diene. Hereby, the electron withdrawing keto-groups of compound **1** cause a low electron density on the respective double-bond, which favours the reaction with the electron-rich cyclopentadiene.[46]

Within the scope of this reaction two different transition states regarding the unsymmetrical dienophile educt may occur. These states are called *endo*- and *exo*-transition states, which lead to the formation of different stereoisomeric products. While in the *exo*-transition state, the substituent is oriented away from the diene π-system, the *endo*-transition state comprises a dienophile which is oriented towards the diene π-system. Due to the fact, that the educt 1,4-anthraquinone (**1**) contains electron withdrawing substituents, the *endo* transition state is more likely to form regarding this reaction, as it is sterically less hindered.[47]

Before the Diels-Alder-reaction shown in Figure 20 could be performed, it was necessary to purify the cyclopentadiene reagent. Cp is a highly reactive compound and therefore prone to dimerization, wherefore it needs to be cracked by heating to 180 °C, followed by a distillation step before carrying out the respective synthesis. A ^{1}H-NMR of cyclopentadiene, which was stored at 0 °C for a period of several months was recorded (Figure 21).

It can be observed that only a small amount of pure cyclopentadiene is present, which did not form the dimerized compound; it needs to be pointed out that dimerization typically occurs much slower at low temperature. This cyclopentadiene-dicyclopentadiene mixture was cracked at 170-180°C to yield a nearly pure cp after subsequent distillation. Looking at Figure *21* the spectrum (blue) of the freshly distilled cp can be observed.

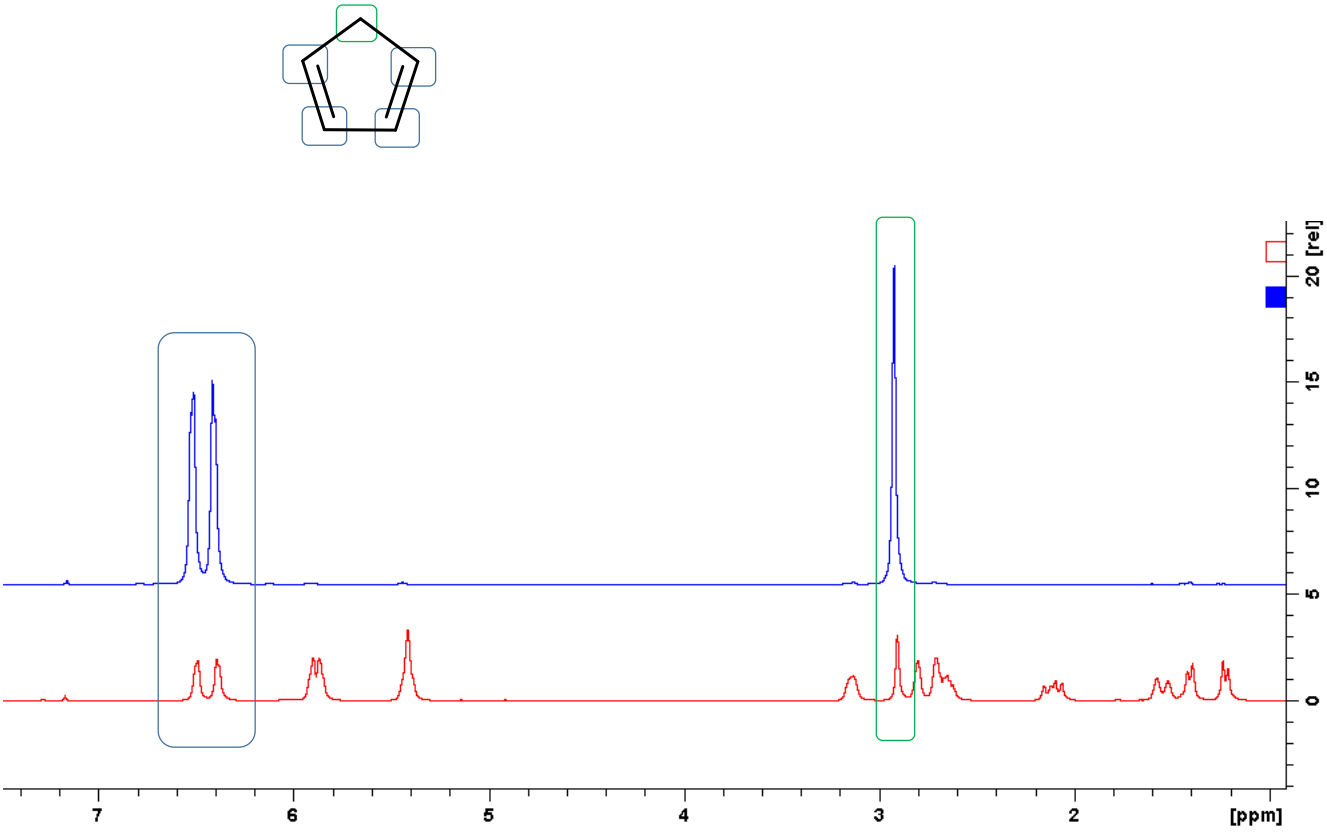

Figure 21: ^{1}H-NMR of pure Cyclopentadiene (blue) and of a cylopentadiene-dicyclopentadiene mixture (red)

After isolation of the pure Cp reagent, the reaction was carried out in a Schlenk flask under nitrogen atmosphere. The reaction progress was monitored via TLC (CH:EE 10+1); after 19 h full conversion of the educt was detected. The crude product was dried under reduced pressure. In order to get rid of unreacted cyclopentadiene, subsequently a column chromatography was performed (CH:EE 10+1). The purified product was obtained as a light orange solid with a yield of 78 %. In general, a yellow color of the product would be expected. The light orange color might indicate remaining traces of quinizarine, which was confirmed by TLC.

Due to the contamination of quinizarine in the product, it was attempted to be further purified by recrystallization according to literature.[48] Hereby, the product mixture was dried under reduced pressure and suspended in ligroin (bp: 60-100 °C). Afterwards, the suspension was filtered and the residue was washed with ligroin. Recrystallization from acetone and evaporation of the solvent under reduced pressure led to isolation of the pure dione. The recrystallization step was repeated twice, resulting of compound **2** in 75 % yield.

3.1.1.3 Deprotonation and Alkylation

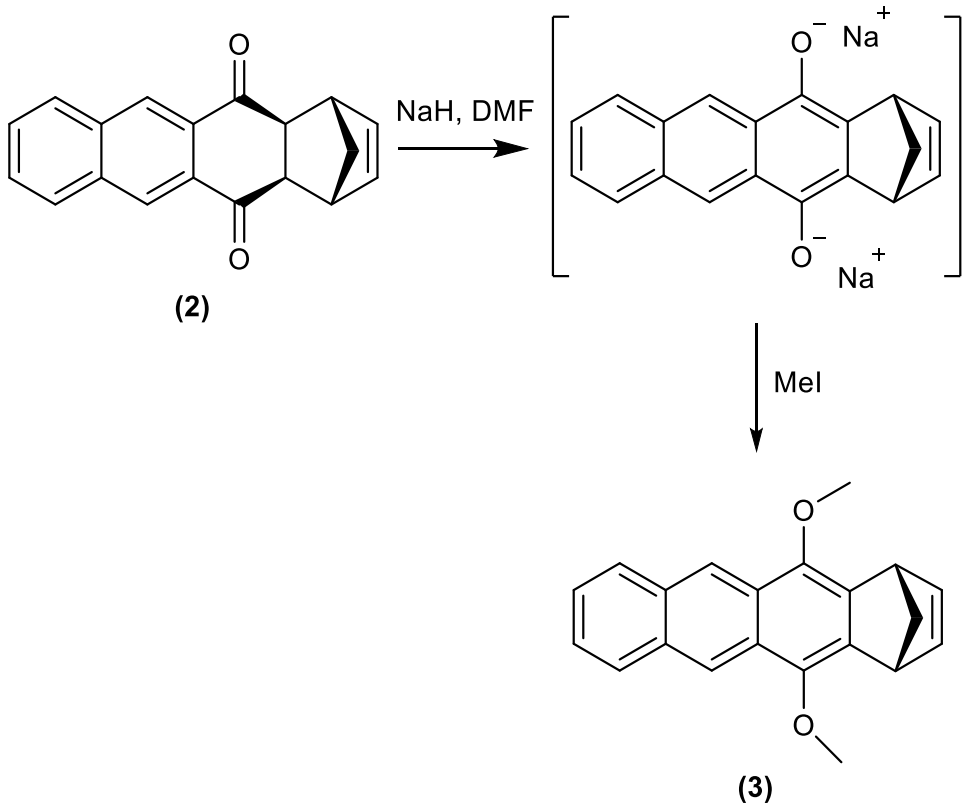

Figure 22: Deprotonation and Alkylation

The third and final step of the synthesis of monomer 1 (**3**) consisted of deprotonation of **2**, using NaH in dry DMF at 80 °C. The reagent is known for its high basicity, making even deprotonation of weak BrØnsted acids possible.[49] If a hydrolysis reaction takes place, NaH is converted into sodium hydroxide (NaOH), a caustic base. Therefore, the NaH is usually stored as a mixture of 60 % sodium hydride in mineral oil under nitogen atmosphere in order to avoid hydrolysis of the reagent. Due to the fact, that NaH is in general insoluble in organic solvents, all reactions occur at the surface of the solid.[50,51] As already mentioned above, NaH is highly prone to hydrolyze, wherefore also the reaction shown in Figure 22 was performed under nitrogen atmosphere in a Schlenk flask, in order to eliminate any traces of moisture or oxygen.

In the first step of this reaction, an enolate-intermediate forms (Figure 22), which was not isolated. This intermediate was alkylated by adding methyl iodide to the reaction mixture; hereby a dark blue color of the reaction mixture could be observed. After a reaction time of several hours, the color changed to dark blue-purple. Although stated in literature[1], full conversion could not be detected after 3 hours. However, after a reaction time of 4.5 h, full conversion of compound **2** was observed via TLC (CH+EE 20:1). The R_f value of the product was found to be 0.43.

In order to proceed with the work-up of the reaction mixture, it was diluted with deionised water, which led to the appearance of a dark brown color. After filtration, the crude product was dried under reduced pressure and purified by column chromatography (CH:EE 20+1). A high yield of 88 % of monomer 1 (**3**) was obtained. Although, the product was purified, the color of the solid was shown to be yellow-orange, while it is stated to be colorless in literature.[1] Reasons for this unexpected obtained color may be impurities of methyl iodide or quinizarine in the purified product. Presence of quinizarine after column chromatography was confirmed via TLC.

3.1.2 Synthesis of the monomer 2 (**5**)

In this section the synthesis of monomer 2 and encountered synthetic difficulties will be discussed. Monomer 2 is also called HBM monomer.

3.1.2.1 Diels-Alder-cycloaddition

The first step for the synthesis of the HBM monomer (**5**) was carried out through a Diels-Alder-reaction. Anthracene was used as the diene to react with norbornadiene, which acts as dienophile. The reaction is shown in Figure 23.

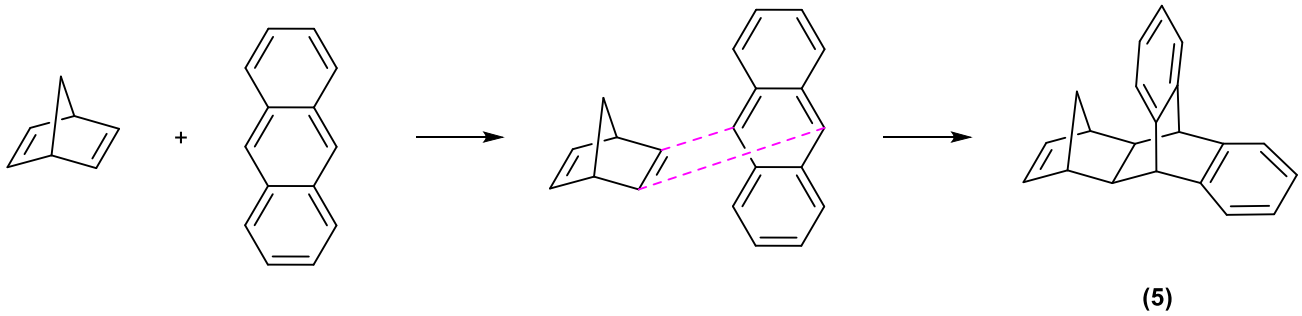

Figure 23: Diels-Alder-cycloaddition to HBM monomer (**5**)

According to literature[38], compound **5** can be prepared by reacting anthracene and norbornadiene at 180 °C for 24 h. After several optimization attempts, a more convenient protocol could be disclosed. In our case, compound **5** was prepared by combining anthracene (1 eq.) and norbornadiene (6 eq.) in a reaction vessel of the Monowave 50 and heating the reaction for 1.5 h at 220 °C. The reaction yielded a slightly brown-colored oil. According to ^{1}H-NMR spectroscopy, almost full conversion of anthracene could be obtained under those conditions (Figure 24).

The unreacted norbornadiene was stripped from the reaction mixture, giving a yellow-white residue. While in literature the residue was purified by recrystallization, a column chromatography was used to completely remove the norbornadiene. The column chromatography was performed using cyclohexane; a yield of 76.2 % of the purified

compound **5** could be obtained. A white crystalline product was isolated, which was stored under nitrogen to avoid possible oxidation.

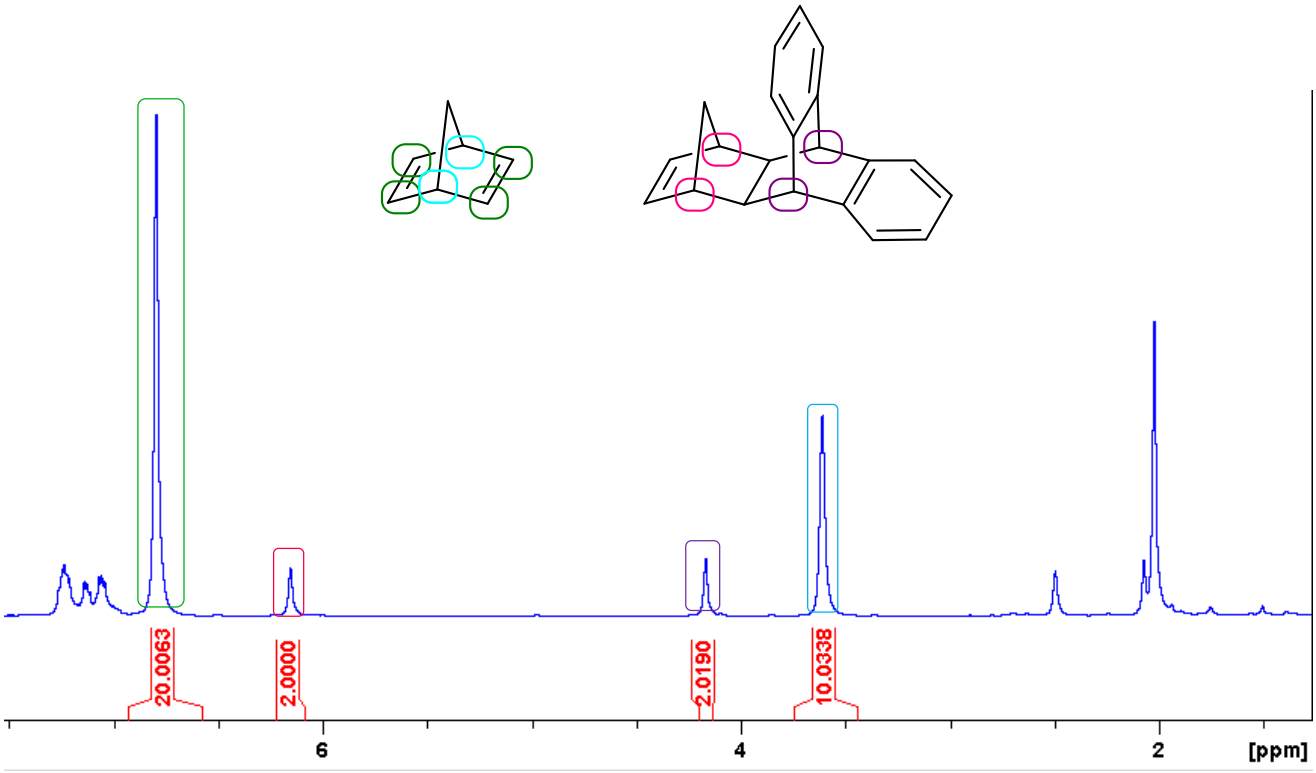

Figure 24: ^{1}H-NMR related to the HBM monomer (**5**)

The excess norbornadiene is necessary to restrict the successive Diels-Alder reaction between the remaining double bond of anthracene and the HBM monomer (**5**) during the reaction. Furthermore, it ensures the complete reaction of anthracene as the unreacted residue is difficult to separate from the product. When the molar ratio of norbornadiene and anthracene is about 6, the reaction can be well controlled with low occurrence of successive Diels-Alder reaction.

The ^{1}H-NMR spectrum of the purified HBM monomer (**5**) is shown in Figure 25.

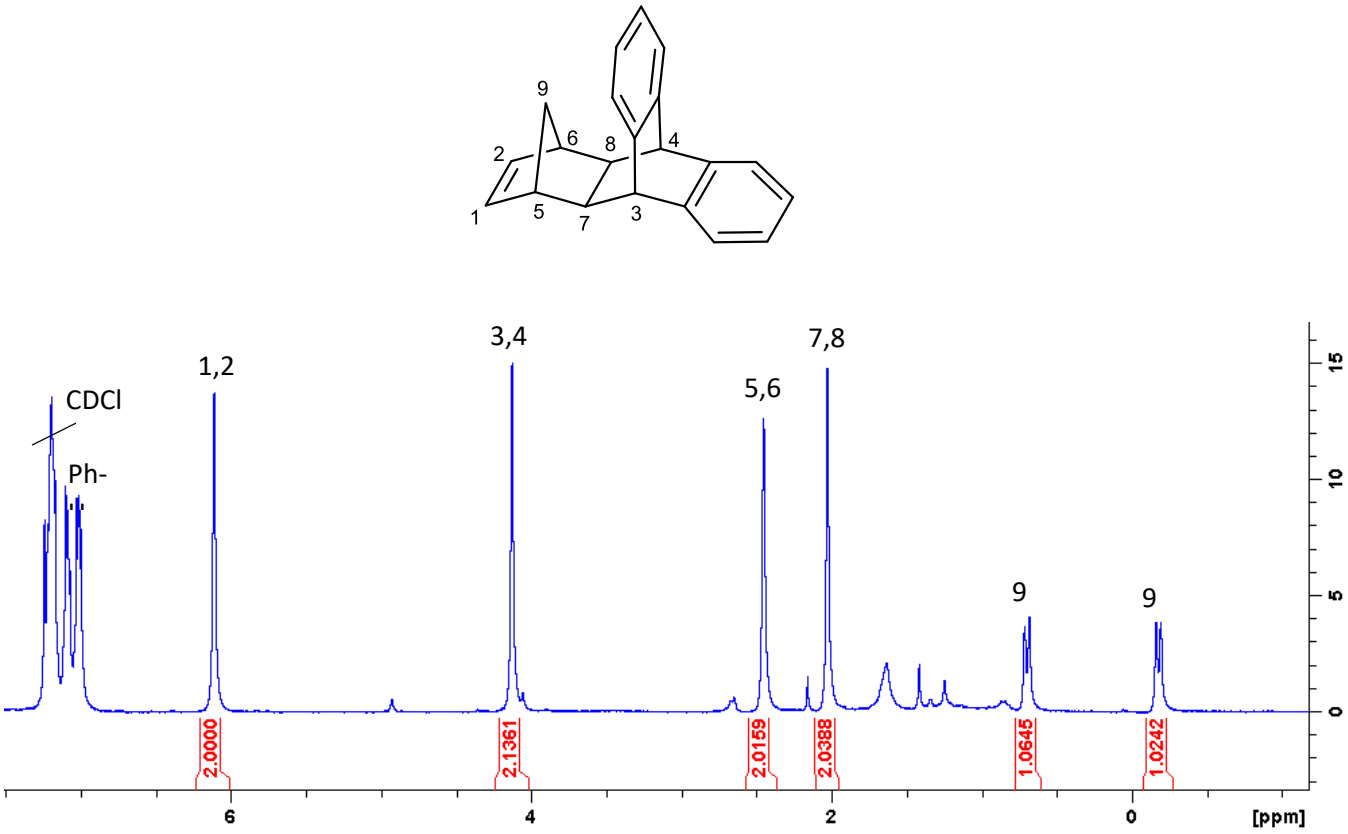

Figure 25: ^{1}H-NMR of the purified HBM monomer (**5**)

3.2 Oligomerization and ROMP

In the following section the oligomerization and subsequent polymerization reactions via ROMP of monomer 1 (**3**) will be displayed. Furthermore, the ROMP of monomer 2 (**5**) will be discussed, whereby no oligomerization step was carried out regarding this monomer.

3.2.1 Oligomerization of monomer 1 (**3**)

A solvent free-melt phase oligomerization of compound **3** was performed under nitrogen atmosphere in the Monowave 50. Generally, solvent-free polymerizations have received significant attention during the last decade. The elimination of organic solvents is primarily driven by environmental concerns and federally mandated emission regulations.[52] In order to carry out the reaction shown in Figure 26, compound (**3**) was heated to 220 °C for 18 h; the resulting product was then directly used for the next synthesis step without further purification. The oligomer (**4a**) was obtained as a solid with a dark brown color.

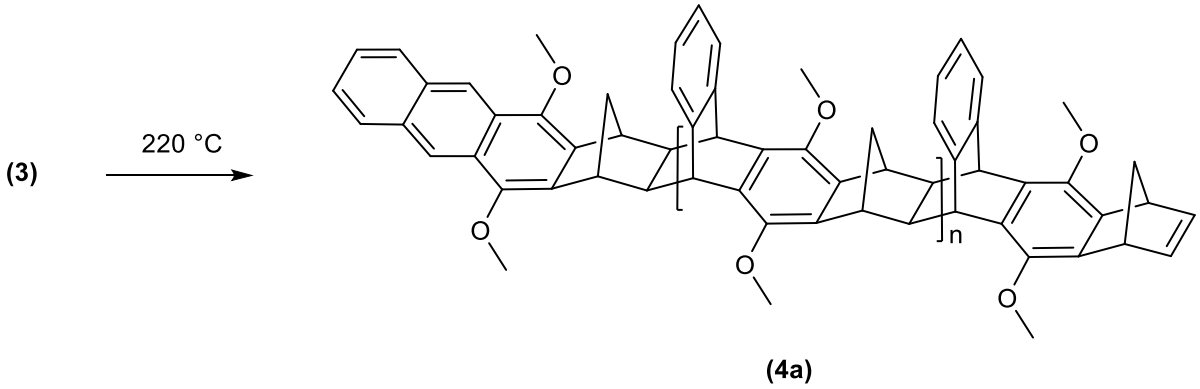

Figure 26: Oligomerization of monomer (**3**)

3.2.2 Ring Opening Metathesis Polymerization (ROMP) of (**4a**)

After the previously described oligomerization reaction, polymerization of the oligomer via ROMP was attempted.

All polymerization reactions were carried out in a Schlenk flask under nitrogen atmosphere. The reactions were performed at room temperature using dichloromethane as a solvent. A Grubbs 3rd generation catalyst (Umicore M31) (structure shown in Figure 29) was used as initiator. The initiator was dissolved in DCM, showing a typical red color. After addition to the reaction mixture, the color changed to orange, indicating the start of the reaction. The reaction was stirred for 48 h to yield a brown-colored polymer (**4b**).

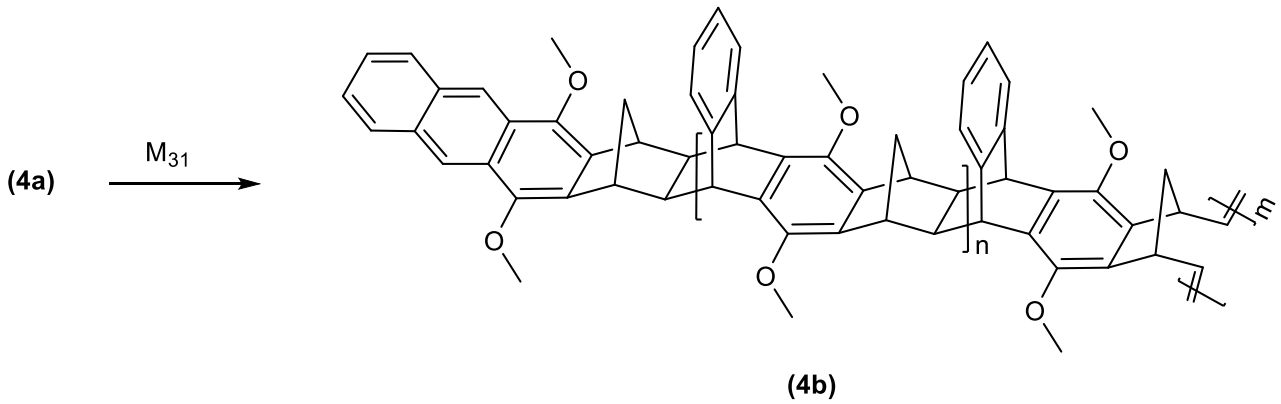

Figure 27: ROMP of oligomer (**4a**) to polymer (**4b**) using the catalyst M_{31}

After detecting total conversion of the monomers by TLC (CH), the polymerization of **4a** was stopped after 48 h by the addition of a quencher. A classical terminating agent used to end-functionalize living polymer chains using 3rd generation catalysts, is ethyl vinyl ether. The general occurring reaction is shown in Figure 28.

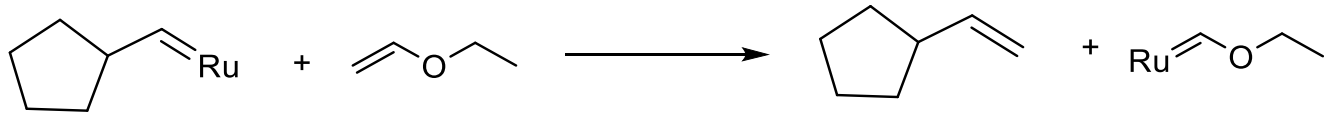

Figure 28: Termination reaction using ethyl vinyl ether

Subsequently, the polymer was precipitated in vigorously stirred methanol and stored under nitrogen atmosphere to avoid oxidation.

The previously described oligomerization and polymerization reactions of compound **3** were carried out twice, whereby the reaction time concerning the ROMP was varied.

The first prepared oligomer and polymer are named (**4a_1**) and (**4b_1**), respectively, whereby, as described above, a reaction time of 48 hours was chosen. The second oligomer is called (**4a_2**), while the corresponding polymer was named as (**4b_2**); regarding these two compounds, the reaction time of the ROMP was set to 20 hours instead of 48 hours.

In order to characterize both synthesized polymers, NMR spectroscopy, GPC and DSC measurements were performed. Furthermore, the porosity was determined via BET surface area analysis. All analyzation data will be displayed and discussed in section *3.5.*

3.2.3 Ring Opening Metathesis Polymerization of monomer 2 HBM (**5**)

The polymerization of HBM (**5**) was performed analogously to polymer (**4b**) using the same initiatior (M31); however a different monomer:initiator ratio of 300:1 was utilized. The reaction was carried out in a Schlenk flask under nitrogen atmosphere, in order to avoid oxidation. The polymerization was finished after 10 min, whereby monitoring of the reaction progress was done via TLC (CH). A norbornene derivate containing bulky hydrocarbon groups was obtained, which is shown in Figure 29. After quenching and precipitation in methanol, the solid was isolated via centrifugation and dried under reduced pressure. The final product (**5**) was stored under nitrogen-atmosphere in a Schlenk flask at room temperature.

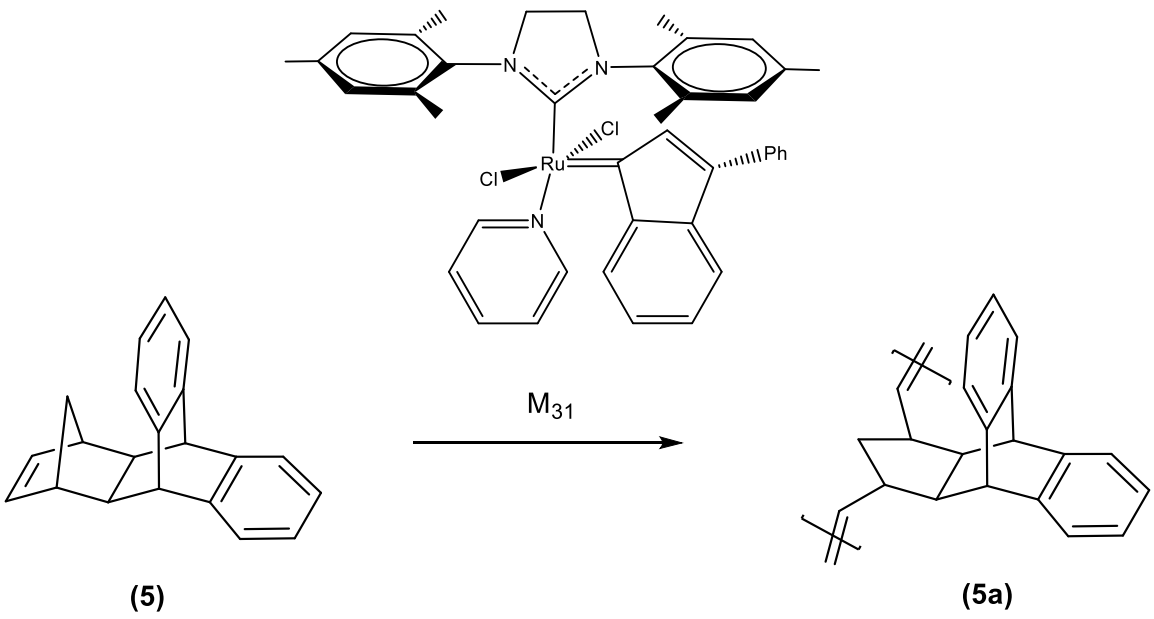

Figure 29: ROMP of the HBM monomer (**5**) leading to polymer (**5a**)

3.3 Additional reactions for the synthesized polymer (5a)

As described in section *3.2.3*, polymer (**5a**) was synthesized via ROMP of monomer 2. Afterwards, it was attempted to hydrogenize this polymer, in order to obtain a polymer which might show enhanced properties for the preparation of polymeric films. The respective hydrogenation reaction will be described in the following.

3.3.1 Hydrogenation of poly(HBM)

Poly(HBM) (**5a**) was hydrogenized (Figure 30), in order to alter the chemical properties and to improve the thermal stability. To enhance the glass transition temperature (T_g), which is the most critical parameter for influencing the thermal stability, a sterically hindered cycloolefin is essential. Usually, these types of polymers are called Cyclic Olefin Polymers (COPs). [37] Such type of polymer can be obtained by hydrogenation of poly(HBM) (**5a**).

The reaction was performed in a Monowave 50 analogously to literature procedure.[37] Unsaturated poly(HBM) was hydrogenized using tripropylamine and *p*-toluenesulfonyl hydrazine by heating up to 120 °C for 16 h under nitrogen atmosphere. Hereby, toluene was used as solvent. After 16 h, the reaction mixture turned to a clear solution. Pouring of the solution into vigorously stirred methanol, led to precipitation of a light brown solid. Subsequently, the polymer was filtered, washed with dist. water and re-dissolved in hot toluene, to repeat the precipitation step. The resulting white polymer (**6**) was obtained with a yield of 91.4 %, dried under reduced pressure and stored under nitrogen atmosphere.

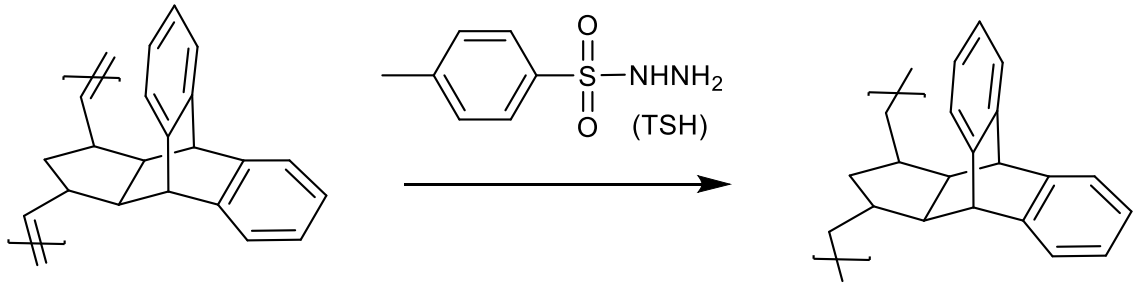

poly(HBM)
(5a)

H-poly(HBM)
(6)

Figure 30: Hydrogenation of poly(HBM) (**5a**) to H-poly(HBM) (**6**)

The hydrogenation shown above was possible due to the high reactivity of the intermediate diimide (NH=NH), which is a species that is able to transfer hydrogen to alkene groups. Tripropylamine was added for the neutralization of p-toluenesulfonic acid, to reduce the formation of unwanted side products.[37]

Complete hydrogenation of polymer (**5a**) to H-poly(HBM) (**6**) was confirmed via ^{1}H-NMR by the disappearance of the signals of the olefinic protons at 5.2-5.6 ppm (Figure 31).

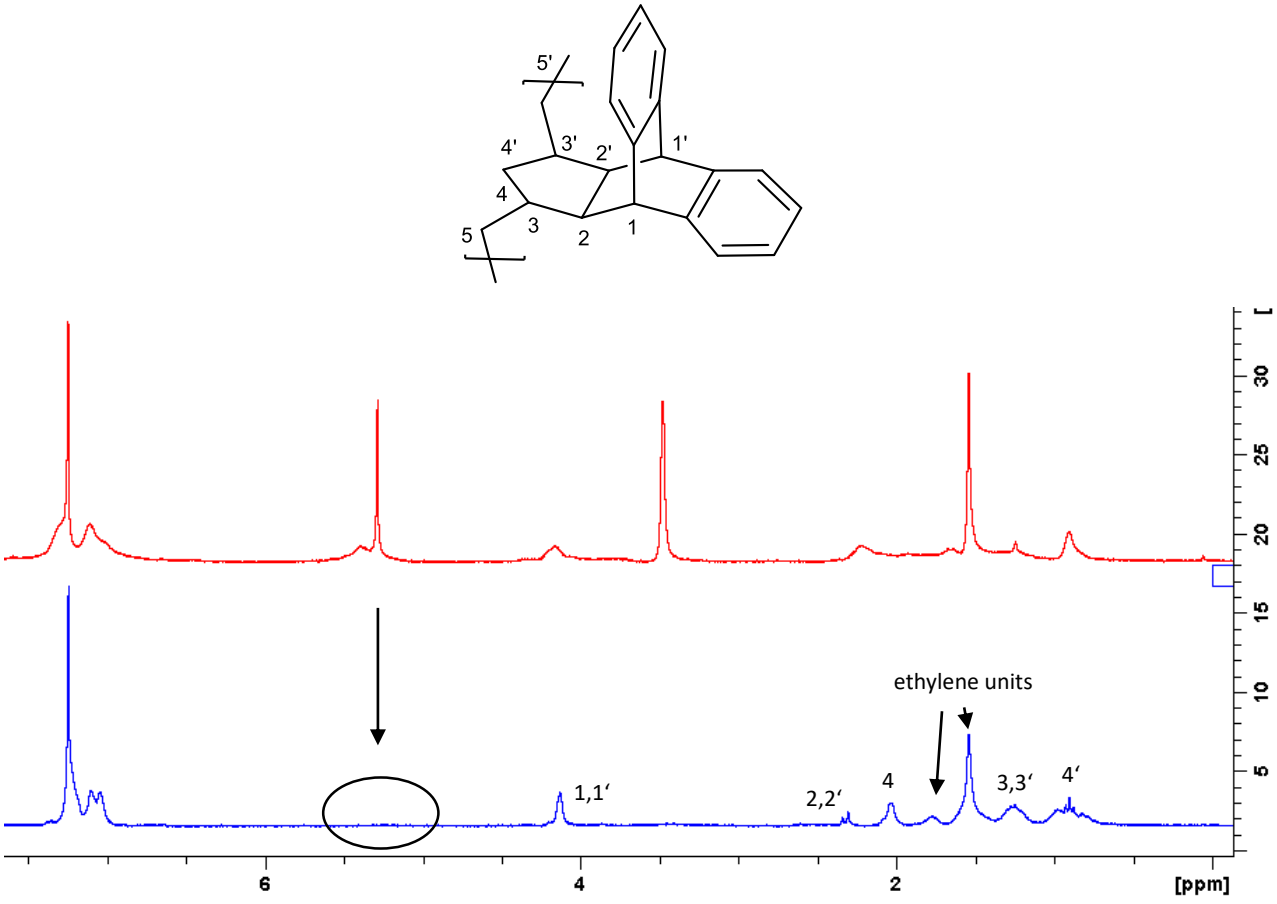

Figure 31: ^{1}H-NMR spectra of poly(HBM) (red) and H-poly(HBM) (blue) in $CDCl_3$

3.4 Synthesis of new porous PolyHIPE materials from monomer 2

Another attempt of this thesis, was to generate a PolyHIPE material from the previously synthesized monomer 2 (**5**).

A PolyHIPE was produced, by using the synthesized HBM monomer (**5**) directly after the reaction in the Monowave 50 in a liquid state. When calculating the required amount of additives for this synthesis, it had to be taken into consideration that norbornadiene was still present in the reaction solution of the monomer. The target was to produce a polymer with a porosity of at least 80 % (see Equation 1). According to equation 1, 7 wt% of the surfactant (Span80) were required. Furthermore, a 2nd generation Grubbs catalyst (M2) in the ratio of 40000:1 was dissolved in 100 µL toluene and added to the reaction mixture. All components were added under vigorous stirring; then water was added dropwise to the reaction mixture. After curring at 40 °C for 2 h in a drying cabinet, the PolyHIPE material (poly(HBM-co-NBD)) was washed with acetone, in order to get rid of contaminants. The foam was dried and stored under nitrogen atmosphere to prevent oxidation.

The idea of producing a polyHIPE of the HBM polymer and the norbornadiene, was to figure out the suitability of the monomer for the formation of polyHIPE structures. In order to characterize the material, ATR-IR spectra of all components were recorded and compared.

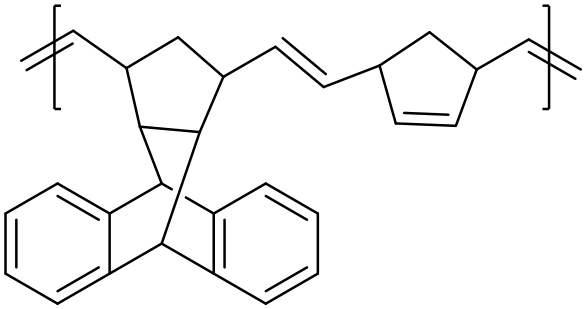

Figure 32: Structure of the poly(HBM-co-NBD)

All the additives were calculated according to an expected porosity of 80 %.

$$porosity\ (0.80) = \frac{m_{H_2O}}{m_{H_2O} + m_{Monomer} + m_{other}} \qquad (1)$$

Equation 1: Calculation of the porosity of the polyHIPE

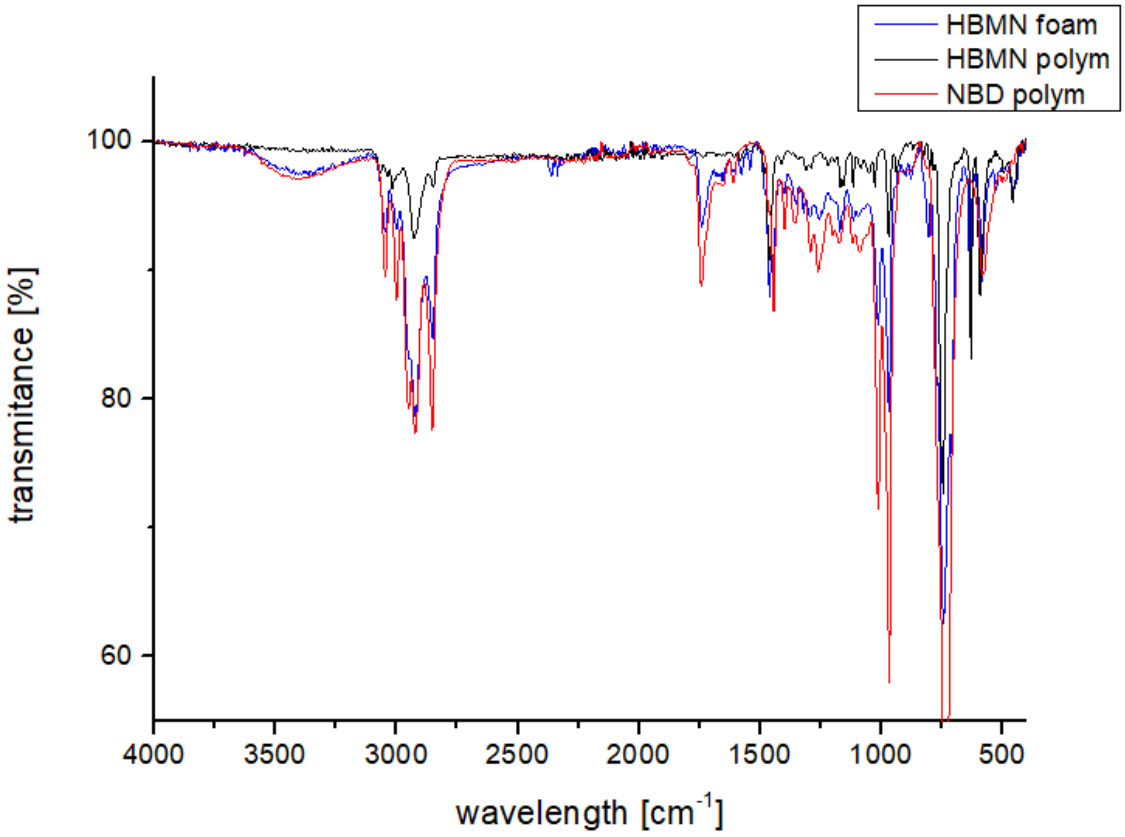

Figure 33:ATR-IR spectra of the polyHIPEs

Looking at the IR-spectrum above, three different spectra of an NBD foam, the previously synthesized polymer (**5a**) (HBMN polymer) and the prepared polyHIPE material (HBMN foam) are shown.

Regarding the spectrum of the HBMN foam and the norbornadiene-foam, the peaks at a wavelength of 3,200-3,700 cm^{-1} and 1,750 cm^{-1} may indicate residues of the surfactant or a slight oxidation of these compounds.

It was assumed that the HBMN foam would show a highly micro porous structure, wherefore it would be expected that an oxidation of this material would take place extremely fast. This assumption could not be confirmed by oxidation experiments; it was shown that oxidation for the prepared NBD foam occurred significantly faster than for the HBMN foam (Figure 34).

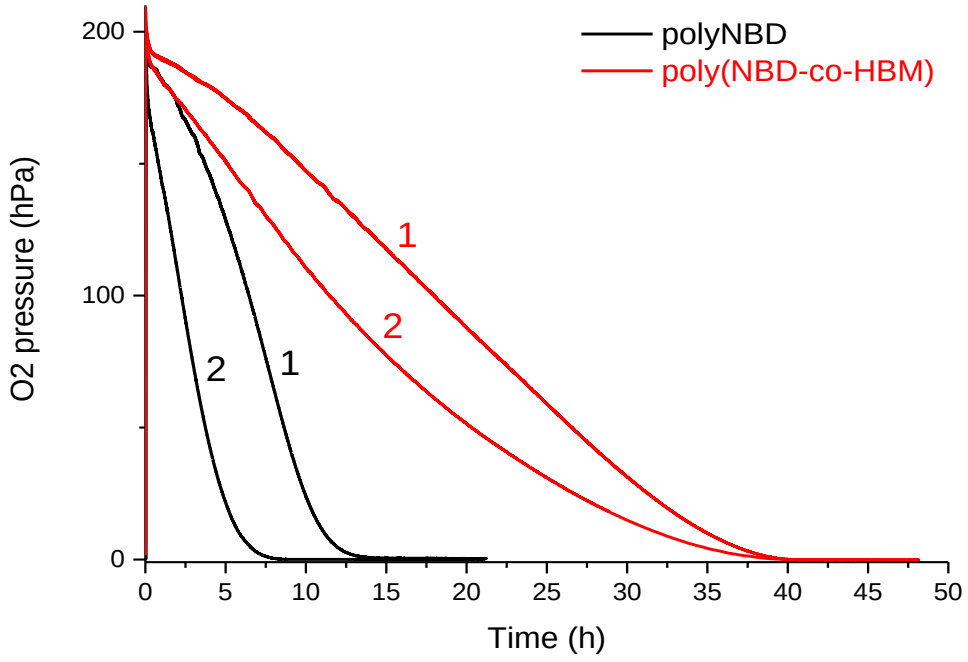

Figure 34: Oxidation of the polyHIPES (poly(NBD-co-HBM) and poly(NBD)

As illustrated in Figure 34, the oxidation of poly(NBD-co-HBM) occurred much slower than in the case of pure poly(NBD). Therefore, it can be assumed that the NBD foam exhibits a higher micro-porous structure than the prepared poly(NBD-co-HBM). However, in order to determine if the synthesized polyHIPE material (poly(NBD-co-HBM)) shows any porous structure, further investigations such as SEM-measurements would have to be performed.

3.5 Characterization of the oligomers and polymers

The oligomers (**4a_1** and **4a_2**) and the respective polymers (**4b_1** and **4b_2**) that were synthesized within the scope of this thesis were characterized via GPC, BET-surface and DSC analysis.

3.5.1 Gel permeation chromatography (GPC) measurement

Gel permeation chromatography, or GPC, is in general a type of size exclusion chromatography, separating analytes on the basis of size. Therefore, this method is commonly used for the analysis of polymers. Regarding the characterization of polymers, the dispersity and the molecular weight have to be considered. As mentioned before, the separation is based on the size or on the hydrodynamic volume (radius of gyration) of the analytes.[53] Separation occurs due to packing of the column with porous beads, which act as the stationary phase. Smaller analytes are able to enter the pores more easily and remain there for a specific amount of time, wherefore their retention time is increased. As a result, small molecules elute last, whereas larger compounds are not able to enter the pores or stay there for a shorter amount of time and are obtained as the first fractions of a gel permeation chromatography.[53,54]

All synthesized oligomers and polymers were characterized by GPC measurement, using THF as solvent, except for the oligomer which was analyzed in chloroform. The recorded molecular weights and their polydispersity index are given in Table 2.

Table 2: GPC data

	M_n [g/mol]	**PDI**
Polymer (4b_1) (48 h)	32,000	1.2
Oligomer (4a_2) (chloroform)	1,200	1.6
Polymer (4b_2) (20 h)	49,000	1.9
HBM polymer (5a)	81,000	1.7
H-HBM polymer (6)	99,000	1.8

Regarding the synthesis of polymer **4b**, oligomerization was done beforehand, in order to achieve a higher polydispersity index, due to increasing structural irregularities. A higher polydispersity index also correlates with a high porosity of the material.

The GPC measurement was performed for both polymers (**4b_1**) and (**4b_2**), whose preparation only differed concerning the reaction time (Figure 35). Polymer (**4b_1**) was synthesized with a reaction time of 48 hours, whereby the reaction time of polymer (**4b_2**) was decreased to 20 hours.

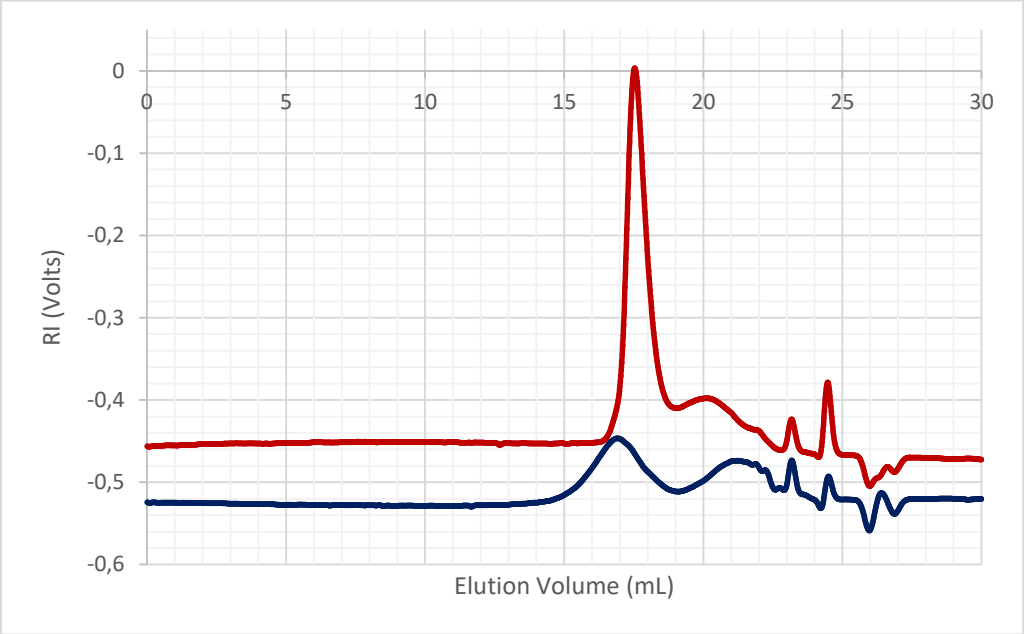

Figure 35: GPC of polymer (**4b_1**) (red) and (**4b_2**) (blue)

Looking at Figure 35, the peak at an elution volume of 23.2 mL can be assigned to the internal standard with a known molecular weight. The peak at 20.2 mL for polymer (**4b_1**) and 21.5 mL for polymer (**4b_2**) is probably due to an unconverted residue of the oligomers (**4a_1**) and (**4a_2**). The peaks which elute at a volume of 17.6 mL (**4b_1**) and 17 mL (**4b_2**) show the respective synthesized polymers.

It can be observed that the curve of polymer (**4b_1**) differs from the graph of polymer (**4b_2**), especially regarding the height of the peak. The difference is probably due to the longer reaction time of 48 hours for polymer (**4b_1**), which allowed for a higher conversion of the oligomer (**4a_1**). As shown in Table 2 the PDI of 1.2 indicates, that polymer (**4b_1**) is well-defined, whereby polymer (**4b_2**) shows a much higher PDI of 1.9. Regarding the peak height

of the oligomer, it can be observed that only small amounts of the oligomer stayed unconverted in case of polymer (**4b_1**) and a higher amount of the educt was found in case of polymer (**4b_2**), where only a small amount of the oligomer was polymerized.

Furthermore, GPC measurements of the HBM polymer (**5a**) and the H-HBM polymer (**6**) were conducted and compared, as shown in Figure 36.

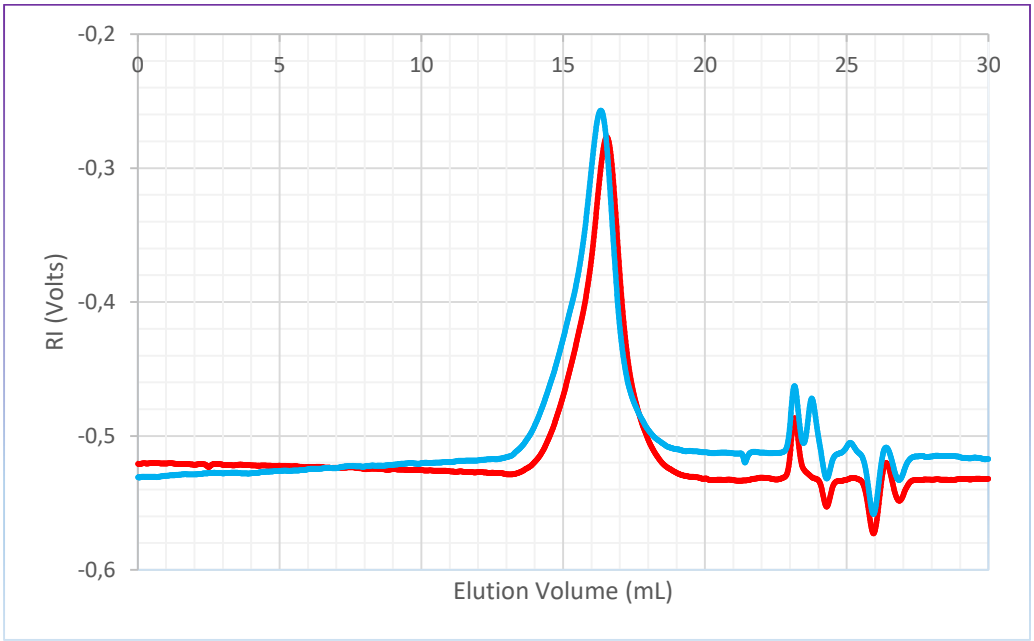

Figure 36: GPC of HBM (**5a**) (red) and H-HBM (**6**) (blue)

Regarding Figure 36, the internal standard elutes at a volume of 23.2 mL. The main peak corresponds to the HBM polymer (**5a**) and the hydrogenated H-HBM (**6**) polymer, with an elution volume of 16.6 mL (**6**) and 16.2 mL (**5a**)**,** respectively. As expected, the molecular weight of the hydrogenated H-HBM is not significantly higher than of the HBM polymer. Both are showing similar PDIs of 1.7 (**5a**) and 1.8 (**6**). The peak at an elution volume of 23.9 mL for polymer (**6**) might be a result of residues of non-hydrogenated polymer, with the consequence of a higher PDI for the H-HBM polymer.

The molecular weights of the HBM and the H-HBM polymer are reported to be 165,000 and 172,000 g/mol in literature, which are quite higher than the measured values shown in Table 2. This circumstance may be caused by the different catalyst-monomer ratio of 500:1, which was used in literature.[37]

3.5.2 Measurement of the specific surface area

The measurement of the specific internal surface area was done by the BET (Brunauer-Emmett-Teller) analysis. BET represents a relatively simple measurement for determination of porosity and surface area, based on gas adsorption. First of all, the samples are dried by applying vacuum or a nitrogen flow under elevated temperatures. Nitrogen is commonly used as gaseous adsorbate. The volume of gas, which is adsorbed to the surface of the sample, is measured at the boiling point of nitrogen (-196 °C). The determined amount of adsorbed gas is directly correlated to the total surface area of the measured polymer. With this method, it is also possible to determine size and volume distribution of micro-pores (0.35-2 nm).[55,56] The measured results and values according to literature of the BET measurements of the synthesized oligomers and polymers are shown in Table 3.

Table 3: Data of the BET measurement

	Specific surface area [m^2/g]
Oligomer (4a_1) and (4a_2)	4[2]
Polymer (4b_1) and (4b_2)	565[2]
HBM	25

According to literature[1], the specific surface area of the oligomers (**4a_1**) and (**4a_2**) was found to be 4 m^2/g and 565 m^2/g for the polymers (**4b_1**) and (**4b_2**)**.** In the respective journal, a Grubbs 2nd generation catalyst was chosen for the polymerization of (**4a_1**) and (**4a_2**). Accordingly, the molecular weight was found to be 340,000 g/mol with a PDI of 2.8. The generation of a high PDI, and an increased structural irregularity lead subsequently to a high porosity. According to literature, the influence of the molecular weight of polymer (**4a_1**) and (**4a_2**) on its surface area was investigated. The expectation was that the degree of polymerization, meaning different molecular weight samples, would increase the surface area. This investigation was performed by varying the amount of Grubbs catalyst, which led to polymers with a different molecular weight of 102,000 and 42,000 g/mol respectively. Although a significantly higher surface area was expected for a higher molecular weight, measurement of the BET surface area showed similar values (558-594 m^2/g) for both polymers. This observation allows the assumption that the topology of polymer (**4b_1**) and

(**4b_2**) is a factor of much higher importance than the molecular weight, regarding the size of the surface area.

The specific surface area of 25 m^2/g of the HBM polymer was determined experimentally. The determined value leads to the conclusion that the polymer shows a micro-porous structure. Because of this micro porous property, it would be expected that oxidation of the analogous polyHIPE sample occurs very fast. However, this assumption was not confirmed via oxidation measurement of the polyHIPE (Figure 34).
For using the polymer as a sensor material, which works at ambient conditions, no oxidation reaction should occur. Therefore, the prepared HBM polymer might be suitable for the application in analytical chemistry, such as methane-sensors.

3.5.3 Differential scanning calorimetry measurement (DSC)

DSC is a technique for measuring the thermal properties of materials, whereby the change of specific physical properties at different temperatures is monitored. DSC measures the heat quantity that is radiated or absorbed excessively by the sample. The basis is the temperature difference between the sample and a reference material.[57]

A DSC measurement was performed for the HBM polymer, in order to determine its glass transition temperature (T_g). This temperature was then compared with literature and glass transition point of the hydrogenated HBM polymer.

Table 4: Data of the performed DSC measurement and of DSC measurements found in literature

	T_g [°C]
HBM	263
HBM [3]	265
H-HBM [3]	221

Due to their amorphous structure, the HBM and the H-HBM polymer exhibit only an apparent (T_g) without showing a specific melting temperature. After the hydrogenation, the (T_g) of the H-HBM polymer subsequently decreases, as shown in Table 4. The lower glass transition

temperature of the hydrogenated polymer H-HBM is probably due to increased flexibility of the polymeric chain by the replacement of the double bonds.[58]

As discussed in section *3.5.1*, the molecular weights of the HBM and the H-HBM polymers in literature, were higher compared to the values that were experimentally determined. Nevertheless, the recorded glass transition temperatures were similar. This fact implicates, that also the T_g is independent from the degree of polymerization.

The T_g for the HBM polymer is very high, which redefines the limits of the thermal properties of COP-materials. As found in literature, the highest T_g value for a synthesised COP-material was determined to be 277 °C. The amorphous structure, the high T_g, and the ability to produce transparent polymer films, enables COP-materials to be promising in practical applications.[38]

The final task of this thesis was to investigate the prepared polymers regarding their suitability as matrix materials of optical oxygen sensors. In general, optical oxygen sensor consist of a luminescence indicator dye, which is entrapped in a polymeric matrix.[59] In order to test the prepared polymers in optical oxygen sensors, a platinum dye ($PtTPTBPF_4$) was used as the indicator dye. For the preparation of the cocktail the dye was dissolved in chloroform and mixed with a specified amount of the polymers to yield a suitable viscosity. The sensor foils were prepared by knife coating of these cocktails onto poly(ethylene glycol terephthalate) supports with a thickness of 2.5 µm. After casting, they were carefully dried overnight at 60 °C. The luminescence was detected with a compact phase fluorometer in water with different oxygen partial pressures (pO_2). Thereby, decay time plots and calibration plots following Stern-Volmer kinetics could be obtained. Subsequently, the decay times and the permeability could be calculated from these plots.

To put the results into perspective, the studied matrix materials were compared to polystyrene, a standard matrix in optical sensors.

3.6 Quenched-phosphorescence oxygen sensing

Optical detection methods offering numerous advantages such as the absence of electromagnetic interferences and the minimally invasive character. The main advantage of optical oxygen sensors is, that they do not consume the analyte. Optodes for oxygen measurement can operate in gases and solutions, with dynamic ranges, over many orders of magnitude. They are very useful for the measurement of air pressure on surfaces or as transducer for enzymatic sensors.[2]

3.6.1 Mechanism of Oxygen Quenching

Oxygen is within the most powerful luminescence quencher. Quenching of phosphorescent dyes, with excited triplet state T_1, and fluorescent dyes, with excited singlet state S_1, is spin- allowed. Quenching of oxygen via energy transfer, is favourable because of their lower energies of the excited states ($^1\Sigma_g^+$ and $^1\Delta_g$) than those of most organic dyes and metal complexes. In general, the oxygen quenching mechanism is rather complex, depending on many factors. The predominant mechanism is based on an electron-exchange Dexter-type energy transfer. The result of quenching fluorescent dyes (D) is the formation of the dye in the triplet excited state or in the ground state.[2,60]

$$D(S_1) \rightarrow D(S_0) + hv$$

$$D(S_1) + O_2(\,^3\Sigma_g^-) \rightarrow D(T_1) + O_2(\,^3\Sigma_g^-)$$

$$D(S_1) + O_2(\,^3\Sigma_g^-) \rightarrow D(T_1) + O_2(\,^1\Delta_g\,)$$

$$D(S_1) + O_2(\,^3\Sigma_g^-) \rightarrow D(S_0) + O_2(\,^3\Sigma_g^-)$$

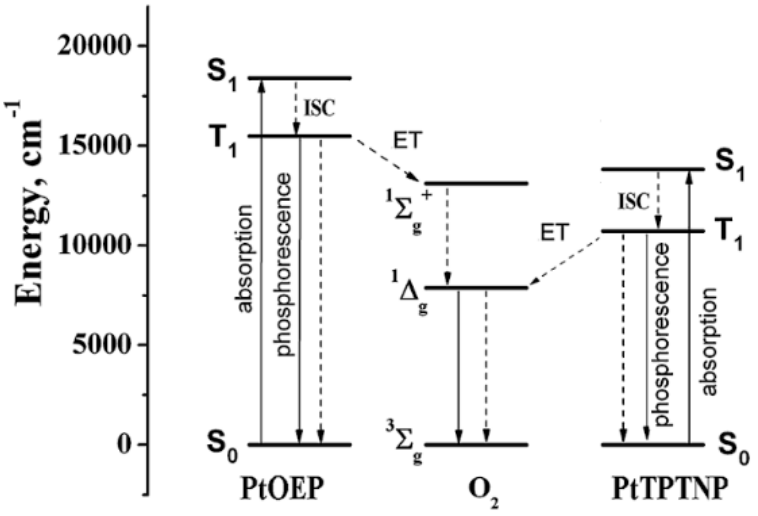

Figure 37: Energy diagram for two phosphorescent oxygen indicators[2]

The triple state of the dye is then deactivated to the ground state:

$$D(T_1) + O_2\left({}^3\Sigma_g^-\right) \rightarrow D(S_0) + O_2({}^3\Sigma_g^-)$$
$$D(T_1) + O_2\left({}^3\Sigma_g^-\right) \rightarrow D(S_0) + O_2({}^1\Delta_g)$$

The dye is deactivated into the ground state and singlet oxygen is formed, for the quenching of phosphorescence:

$$D(T_1) + O_2\left({}^3\Sigma_g^-\right) \rightarrow D(S_0) + O_2({}^1\Sigma_g^+)$$
$$D(T_1) + O_2\left({}^3\Sigma_g^-\right) \rightarrow D(S_0) + O_2({}^1\Delta_g)$$

Only the formation of singlet oxygen in the ${}^1\Delta_g$ state (for PtTPTNP, Figure 37) or in both ${}^1\Delta_g$ and ${}^1\Sigma_g{}^+$ (for PtOEP) is possible, depending on the triplet energy of the dye. The $O_2({}^1\Sigma_g{}^+)$ deactivates very fast into the $O_2({}^1\Delta_g)$ state. Singlet oxygen represents the main product for all these processes.

The quenching behaviour for dissolves dyes is according to the Stern-Volmer equation:

$$\frac{I_0}{I} = \frac{\tau_0}{\tau} = 1 + k_q \tau_0 [O_2] = 1 + K_{SV}[O_2] \qquad (2)$$

Equation 2: Stern-Volmer equation

Where $I_0(\tau_0)$ and $I(\tau)$ are describing the luminescence intensity (decay time) in the absence and presence of oxygen. K_{SV} is the Stern-Volmer constant, and k_q the bimolecular quenching constant. The term $[O_2]$ may be replaced by the partial pressure pO_2.
Only phosphorescence indicators will provide the required resolution in common polymeric materials, because the diffusion of oxygen is slower in polymers compared to the diffusion in solution. The major requirement for optical oxygen sensors is, that the matrix has to be permeable to oxygen, while being impermeable to other potential quenchers.
The decay time of phosphorescence can vary from several microseconds to hundreds of milliseconds.[2,61]

3.6.2 Indicator

A platinum(II) meso-tetra(4-fluorophenyl) tetrabenzoporphyrin phosphorescence oxygen indicator dye was used for the O_2 sensing of the poly(HBM) (**5a**), the poly(H-HBM) and the polymer **4b**. The structure of the used indicator is shown in Figure 38. It was necessary to choose an indicator, which is immobilized in the matrix, or absorbed on/covalently coupled to the surface of the porous materials. The polymeric matrix acts as solvent and as support for the dye. The compatibility of the polymer and the dye is important, which means they should not differ significantly in polarity. Sensors prepared from crystalline polymers may tend to build cracks, or detach from the support

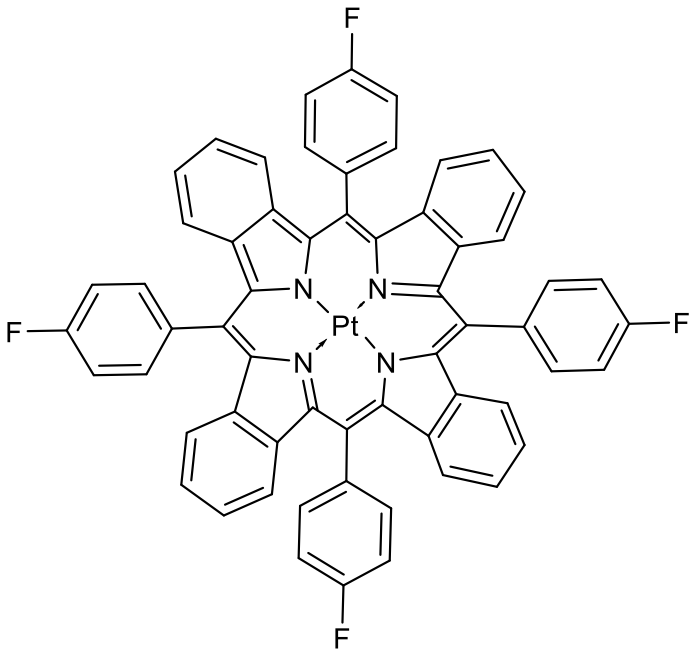

Figure 38: PtTPTBP modified with fluoride substituents

Sensitivity and the dynamic range of optical oxygen sensors is determined by the phosphorescence decay time of the indicator τ_0 and the oxygen permeability. This can be presented as a product of oxygen solubility in the polymer and the diffusion coefficient.[2]

3.6.3 Measurement

The luminescence phase shifts were measured with a compact phase fluorometer from Pyroscience. The measurement was done in water. The excitation was performed with the light of a 624 nm LED, modulated at a frequency of 4,000 Hz. The excitation-light was guided to the sensor film by an optical fibre. A RG9 emission filter (Schott) were used and the luminescence was guided back to the photodiode. Sensor foils were fixed to the end of the fibre with a screwable cop.

With a cryostat (ThermoHaake DC50) the temperature was controlled to 25 °C and a gas mixing device (Voigin) was used to obtain a gas mixture of N_2 and compressed air, which was bubbled through the solution. The oxygen partial pressure (pO_2) was modified by a continuous increase every eight minutes as shown in Table 5.

The luminescence lifetime was measured every 5 seconds, to get enough data points for further evaluation.

Table 5: Oxygen partial pressure adjusted with the gas mixing device

Time [min]	**pO_2 [kPa]**
0	0
8	0.494
16	0.988
24	1.976
32	3.952
40	7.904
48	19.76

The measurement was running for more cycles to select the most effective ones, for the further calculations. Because of some gas bubbles set to the sensor film, disruptions of the measurements, were caused. First of all, the phase shifts was plotted against the time [s] shown in Figure 39.

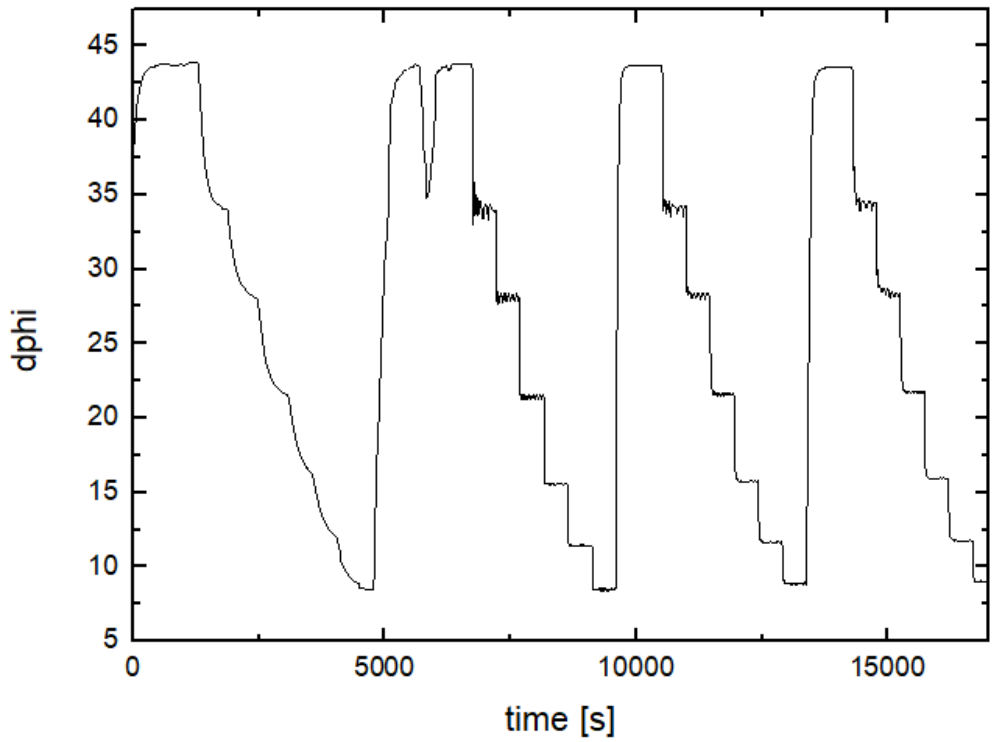

Figure 39: Phase shift vs. time [s] of polymer **4b**

3.6.3.1 Decay time plots

With the measurement of more cycles the data got more accurate. The phase shift of every associated oxygen partial pressure (pO_2) was noted over three cycles and an average was generated. These average was plotted against the oxygen partial pressure (pO_2) as shown in Figure 40.

Table 6: Average of the phase shifts of polymer **4b**

	Phase shift, cycle 1	**Phase shift, cycle 2**	**Phase shift, cycle 3**	**Average**
0	43.76	43.70	43.60	43.69 ± 0.081
0.494	34.01	34.18	34.55	34.25 ± 0.28
0.988	28.21	28.40	28.37	28.33 ± 0.10
1.976	21.51	21.59	21.81	21.64 ± 0.16
3.952	15.56	15.76	15.94	15.75 ± 0.19
7.904	11.37	11.63	11.75	11.58 ± 0.19
19.76	8.560	8.900	8.950	8.803 ± 0.21

The τ values of the HBM and the H-HBM polymer were calculated similarly and plotted in Figure 41and Figure 42.

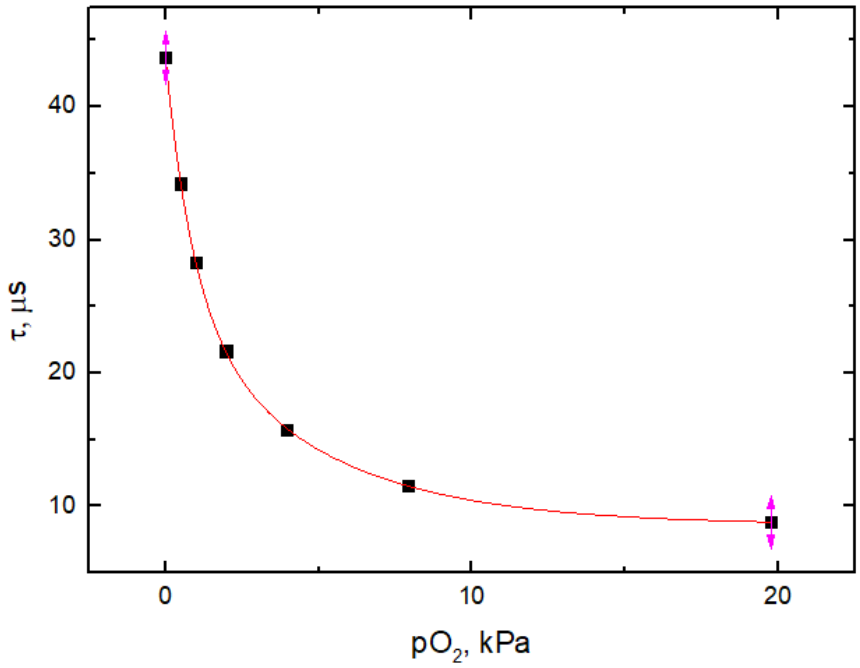

Figure 40: Decay time plot for polymer **4b**

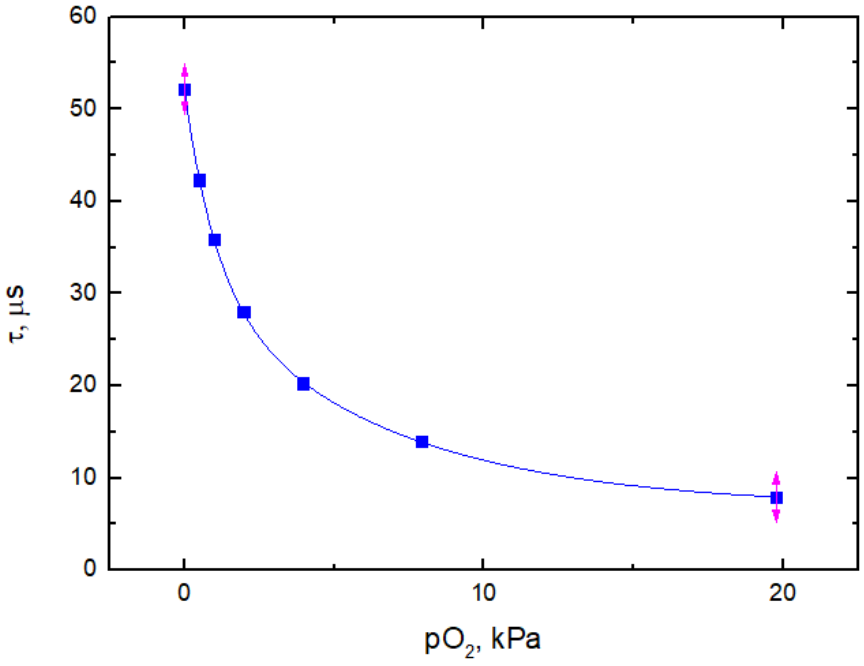

Figure 41: Decay time plot for the HBM polymer

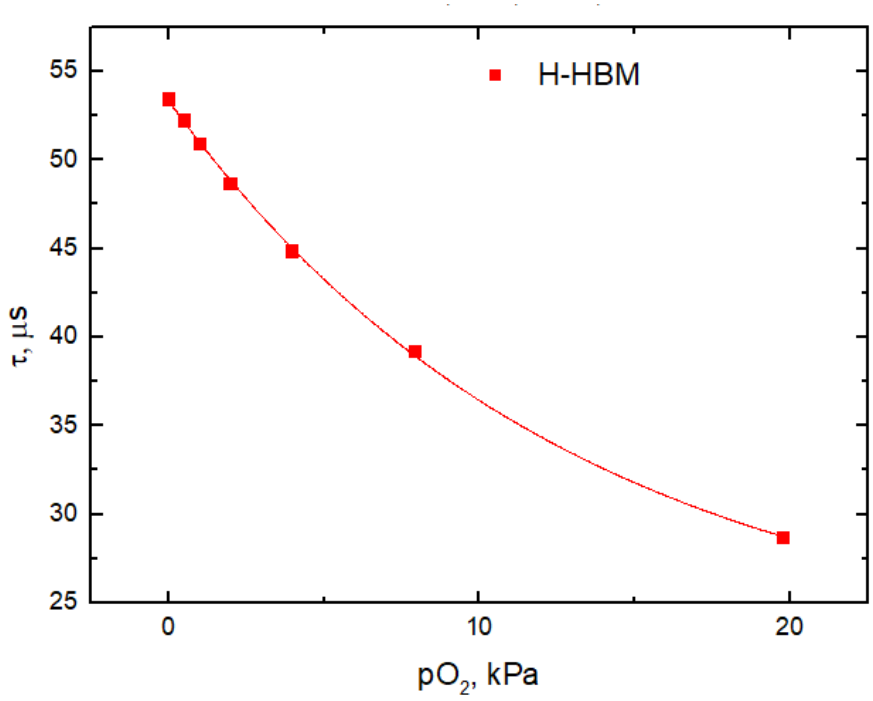

Figure 42: Decay time plot for the H-HBM polymer

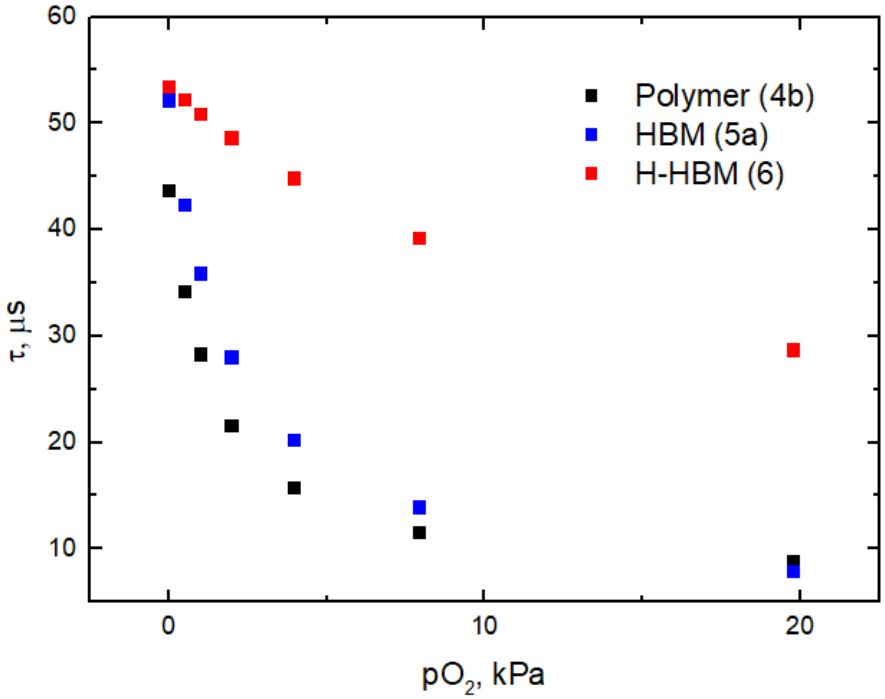

Figure 43: Decay time plots for polymer **4b**, **5a** and **6**

3.6.3.2 Calculation of the decay times

The decay times of the polymers were calculated by the following formula:

$$\tau_0 = \frac{tan\varphi}{2\pi f} \qquad (3)$$

Equation 3: Calculation of the decay times τ_0

Table 7: Calculated of the decay times τ_0

	τ_0 [µs]
Polymer (4b)	38.01
HBM	51.20
H-HBM	53.70
Polystyrene	52.55[62]

Polymer **4b** shows the lowest decay time with 38.01 µs, maybe caused by aggregation. The decay times of the dye in the HBM and the H-HBM polymer is comparable to the decay time in polystyrene.

3.6.3.3 Stern- Volmer calibration plots

By plotting the decay time in the absence of the quencher τ_0 divided by the decay time in the presence of the quencher τ against the quencher concentration pO_2, plots were generated following Stern-Volmer kinetics, shown in Equation 2. The Stern-Volmer constant, K_{SV} expresses therefore the sensor sensitivity, which is directly influenced by its oxygen permeability.

The Stern-Volmer calibration plots of polymer **4b** and of the HBM polymer are nonlinear, which is quite common for optical sensors.[63] A calibration behaviour like this can be described by a two-site model (Equation 4), with K_{SV1} and K_{SV2}, which are two different Stern-Volmer constants, and F being the distribution coefficient.

In an ideal quencher system, there would be a linear relationship between $\frac{\tau}{\tau_0}$ and the oxygen partial pressure.[2,61]

$$\frac{\tau}{\tau_0} = \frac{f}{1 + K_{SV1} * pO_2} + \frac{1 - f}{1 + K_{SV2} * pO_2} \qquad (4)$$

Equation 4: Stern-Volmer 2 site model

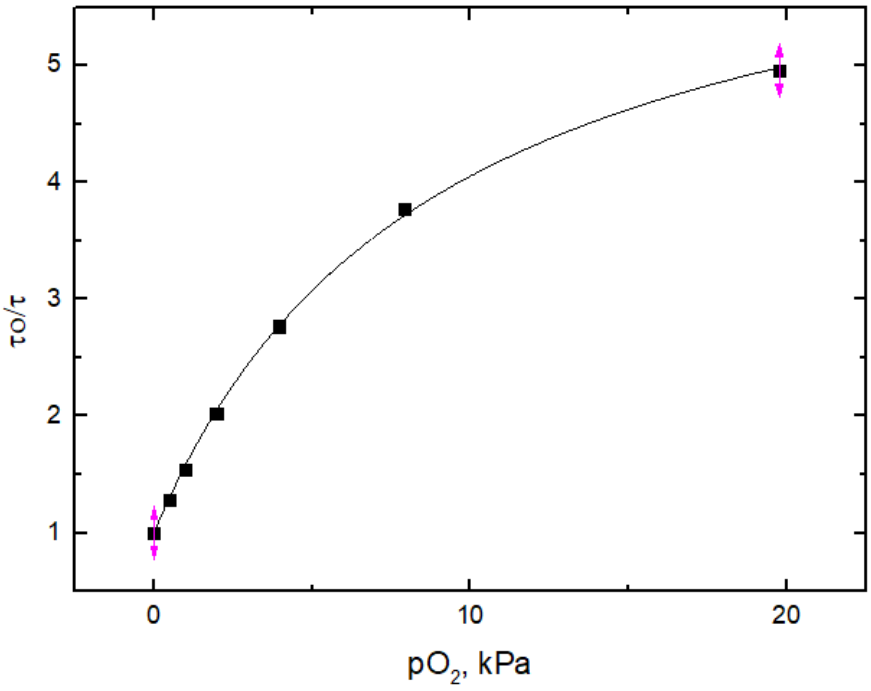

Figure 44: Stern-Volmer calibration plot of polymer **4b**

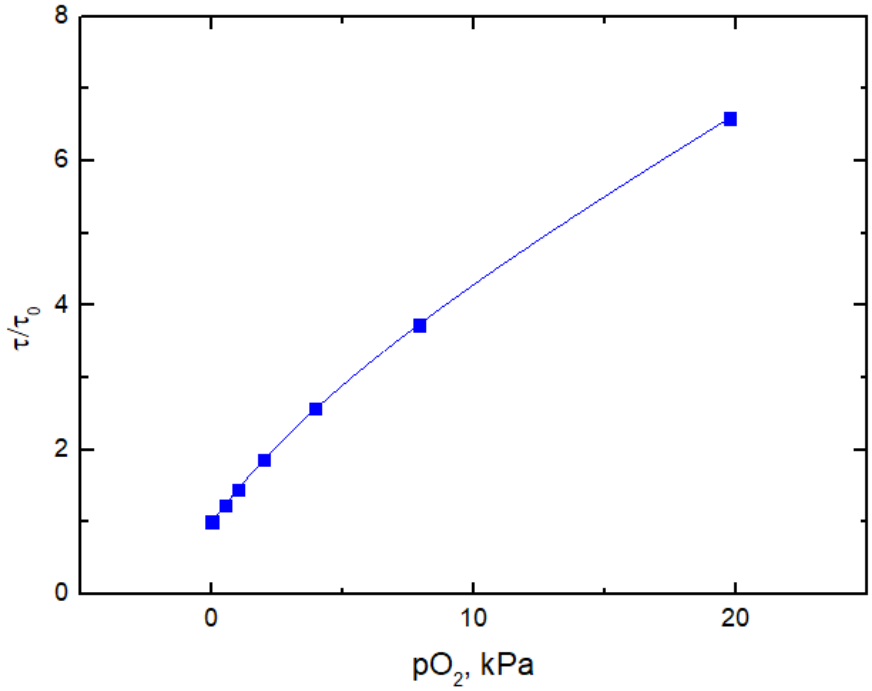

Figure 45: Stern-Volmer calibration plot of the HBM polymer

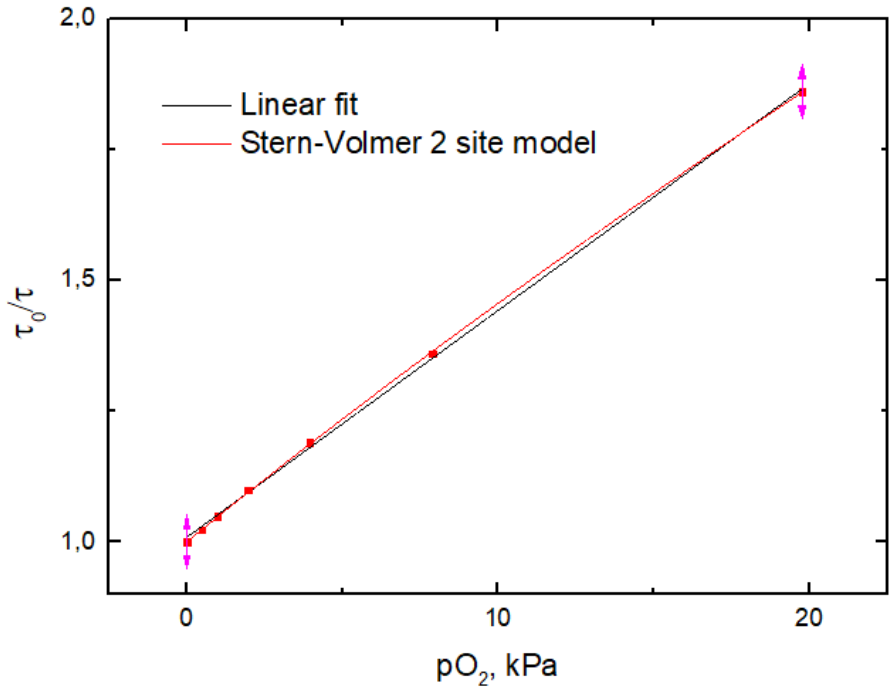

Figure 46: Stern-Volmer calibration plot the H-HBM polymer

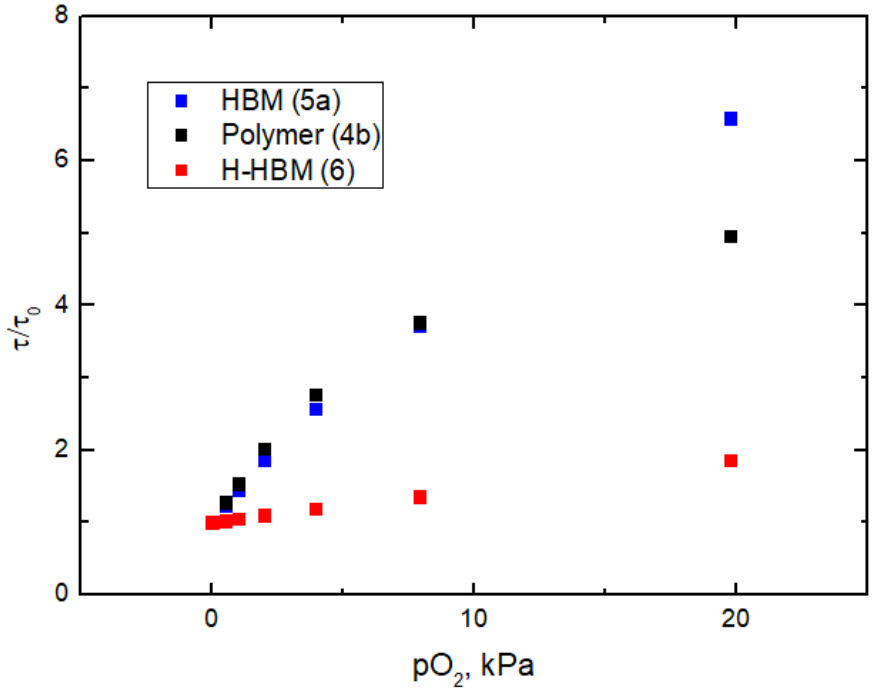

Figure 47: Stern-Volmer calibration plot of **4b**, **5a** and **6**

The calculated constants are presented in Table 8. For the H-HBM polymer, a linear fit, with R^2= 0.999, and a Stern-Volmer two site model were used.

The second constant K_{SV2} can be calculated by K_{SV1} multiplied by the factor m.

Table 8: Stern-Volmer constant

	Stern-Volmer 2 site model			**Linear fit**
	K_{SV1} [kPa^{-1}]	m	F	K_{SV}
Polymer (4b)	0.759 ± 0.047	0 ± 0.0051	0.85 ± 0.014	-
HBM polymer	0.580 ± 0.0092	0.077 ± 0.0032	0.84 ± 0.0068	-
H-HBM polymer	0.058 ± 0.0011	0.18 ± 0.031	0.80 ± 0	0.043 ± 0

The results can be compared to polystyrene, which shows moderate oxygen permeability, but is one of the most commonly used matrices due to low costs, good solubility in various organic solvents, good chemical stability and optimal sensitivity in ambient conditions.[2]
$PtTPTBPF_4$ in polystyrene has a Stern-Volmer constant K_{SV} of 0.174 kPa^{-1}, therefore the H- HBM polymer possesses a three times lower permeability than polystyrene.[62]
In contrast, polystyrene has a three times lower permeability to the HBM polymer, and a four times lower permeability to polymer **4b**, which has the highest Stern-Volmer constant.

3.6.3.4 Photobleaching test

By increasing dramatically, the dose of the illumination from 1 mp/5 seconds to 1 mp/1 second and an integration time increasing eight-fold, the illumination dose is risen 50 fold. With this modification the photochemical alteration of the dye is measured. In general, the alteration is measured until a dye, or fluorophore molecule is permanently unable to fluoresce, caused by cleaving of covalent bonds or reactions between surrounding molecules with the fluorophore.[64] These irreversible modifications can be related to the transition from a singlet state to the triplet state of the fluorophores or the decomposition of the polymer produces a quenching species.
The HBM and the H-HBM polymer were analysed by photobleaching over three cycles. Therefore, the phase shifts were again plotted against the time [s] as shown in Figure 48 and Figure 49. In both cases a decrease of the phase shift with the time can be recorded, which indicates that both sensors are not long-term stabile. The H-HBM polymer shows a considerably higher degradation than the HBM polymer.

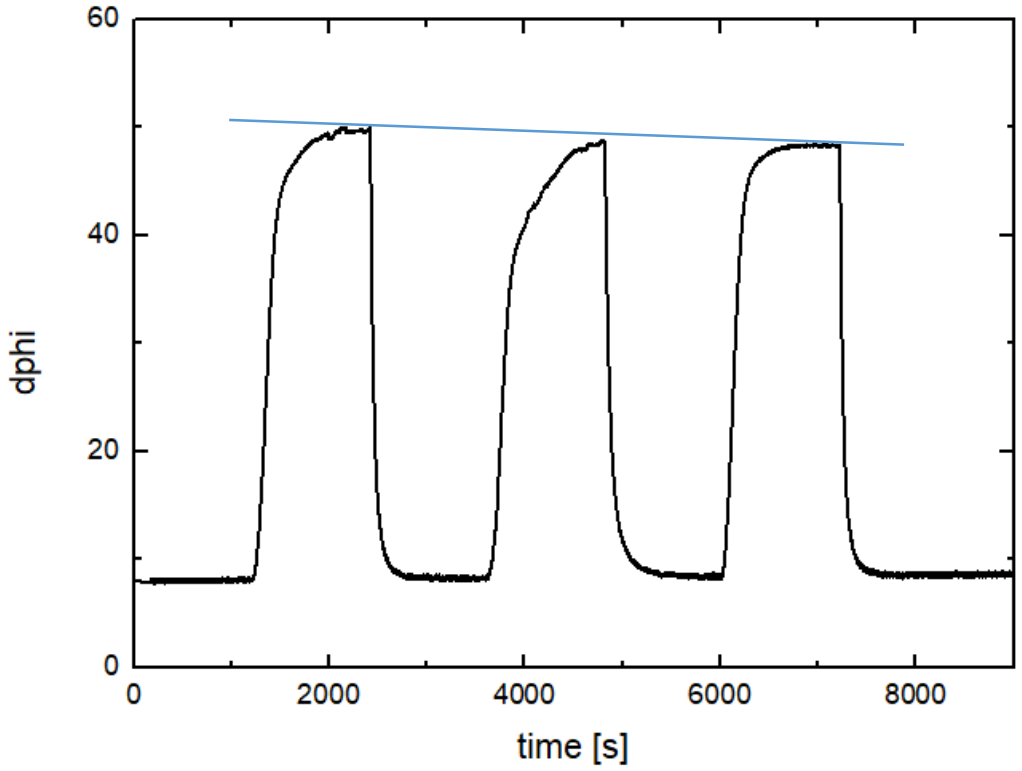

Figure 48: Photobleaching test of the HBM polymer

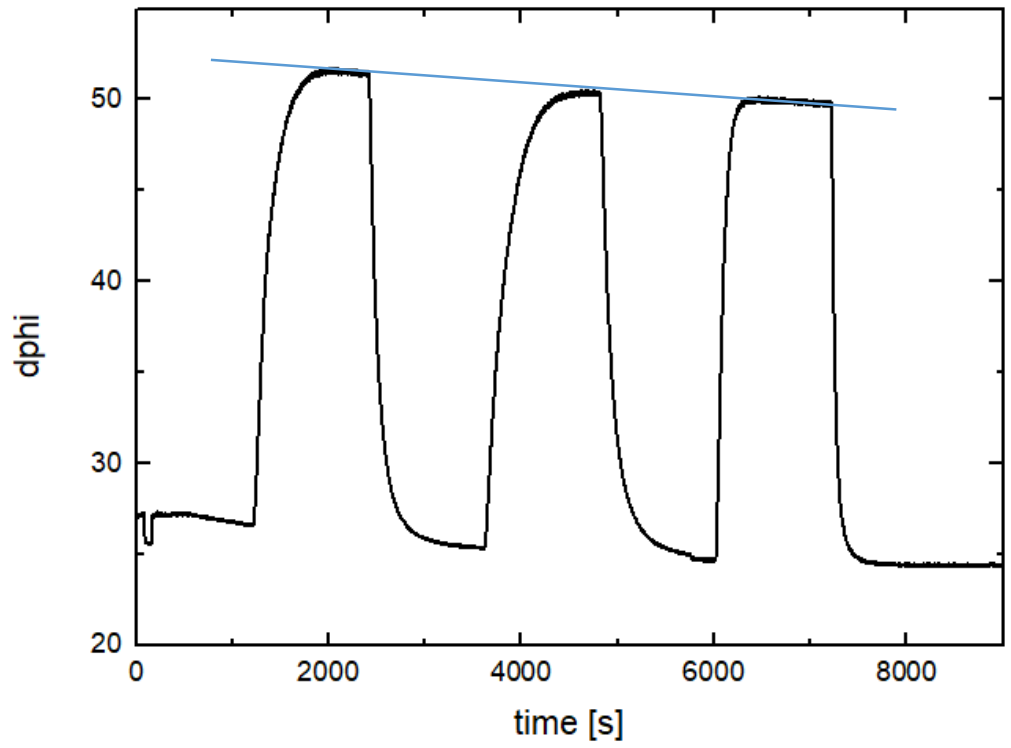

Figure 49: Photobleaching test of the H-HBM polymer

4. Conclusion and Outlook

Within the scope of this Master's thesis two monomers were successfully isolated. The first monomer was prepared through a three step synthesis, leading to 5,12-dimethoxy-1,4-dihydro-1,4-methanotetracene (**3**). The second monomer (**5**), exo-1,4,4a,9,9a,10-hexahydro-9,5(1',2')-benzeno-1,4-methanoanthracene (HBM), was prepared through a Diels-Alder reaction of anthracene with 2,5-norbornadiene.

These monomers were used as starting materials for the preparation of two porous organic polymers through ring opening polymerization (ROMP). Compound **3** was oligomerized prior to that (oligomer **4a_1**) and then subsequently polymerized (**4b_1**), whereby compound **5** was polymerized without any oligomerization step to polymer **5a**. Thereby, the oligomerization and polymerization of compound **3** was done twice (**4a_2** and **4b_2**) with a different reaction time of the polymerization, set to 20 hours instead of 48 hours. Afterwards, it was attempted to hydrogenize polymer **5a**, in order to alter the chemical properties and improve the thermal and oxidative stability.

The synthesised polymers were characterized via GPC measurements and molecular weights of 32,000 g/mol for polymer **4b_1**, 49,000 g/mol for polymer **4b_2**, 81,000 g/mol for the HBM polymer (**5a**) and 99,000 g/mol for the hydrogenated HBM polymer (**6**) could be determined.

Nitrogen absorption measurements were done for the HBM polymer (**5a**) and a specific surface area of 25 m^2/g was determined. This value leads to the conclusion that the polymer shows a micro-porous structure. Due to this assumption a polyHIPE of the HBM monomer (**5**) was prepared with the expectation that an oxidation of this material would take place extremely fast. This could not be confirmed by oxidation experiments; it was shown that oxidation for the prepared HBM foam occurred slower than expected. However, in order to determine if the synthesized polyHIPE shows any porous structure, further investigations such as SEM-measurements would have to be performed.
According to literature[1], polymer **4b_1** and **4b_2** are showing high surface areas of 565 m^2/g.

Additionally, a very high glass transition temperature of 263 °C, of the HBM-polymer (**5a**), was measured via DSC, which redefines the limits of the thermal properties of porous organic polymers.

Furthermore, the polymers were characterized by a quenched- phosphorescence oxygen sensing to measure the oxygen permeability of the matrices. The results can be compared to polystyrene, which shows moderate oxygen permeability.[2]
The hydrogenated HBM polymer (**6**) possesses a three times lower permeability than polystyrene. In contrast, polystyrene has a three times lower permeability to the HBM polymer (**5a**) and a four times lower permeability to polymer **4b_1**.

In future, further investigations concerning the synthesis of porous organic polymers will be carried out, in order to find suitable polymers for an efficient application in gas storage.

5. Experimental Part

5.1 Chemicals

All chemicals have been purchased from Sigma-Aldrich, TCI or ABCR and were, unless specified otherwise, used as received. Used solvents for reactions, work-up and purification were of analytical grade and also used as received. For the purification of the synthesised compounds column chromatography was performed with different mixtures of cyclohexane and ethylacetate as mobile phase. Silica gel 60 was used as stationary phase.

5.2 Methods of Characterization

5.2.1 Thin layer chromatography

For thin layer chromatography (TLC) silica-gel plates on aluminium (Kieselgel 60 F_{254} Merck 5554) were used. The detection was done using a UV-lamp (254 nm) or a potassium permanganate solution (1 wt% $KMnO_4$ dissolved in water). As eluent different mixtures of cyclohexane and ethylacetate as the mobile phase were used.

5.2.2 Infrared spectroscopy

The infrared-spectroscopy measurements were taken on an Alpha FT_IR spectrometer from Bruker with the Platinum ATR single reflection diamond ATR module. The results were presented in cm^{-1}.

5.2.3 NMR- spectroscopy

^1H-NMR and ^{13}C-NMR spectra were recorded on a Bruker Ultrashield 300. The spectra were obtained at 300.36 MHz for ^1H and 75.53 MHz for ^{13}C, in $CDCl_3$. The chemical shifts for the ^1H-spectra are reported in points per million (ppm) relative to the singlet of $CDCl_3$ at 7.26 ppm. The chemical shifts for the ^{13}C-spectra are reported relative to the triplet of $CDCl_3$ at 77.16 ppm. The multiplicity of the peaks is specified with singlet (s), doublet (d), triplet (t), quadruplet (q), multiplet (m) and broad (b).

5.2.4 Differential Scanning Calorimetry DSC

The DSC measurement of the poly(HBM) (**5a**) was performed by Josefine Hobisch on

a DSC 8500 instrument from Perkin Elmer. Thereby, the glass transition temperature (T_g) was read as the middle of change in heat capacity. Heating rates were 10°C/min.

5.2.5. Gel Permeation Chromatography GPC

The GPC measurements were of **4a**, **4b**, **5a** and **6** were performed by Josefine Hobisch. Thereby, the weight average of molecular mass (M_W) and the polydispersity indices (PDI) were determined. All measurements were carried out on a GPC device from WGE Dr. Bures (SEC 3010) Two MZGel SDplus Linear, 5 µ, 30 cm columns were used and a refractive index detector. As solvent THF (1 mL/min) was used, excepted from **4a**, which was carried out in chloroform.

5.2.6 Oxidation measurement of the polyHIPE

Oxygen measurement on the poly(NBD-co-HBM) polyHIPE was recorded by a octical oxygen meter FireStingO2 combined with a contactless oxygen sensor (sensor spot) from PyroScience. The oxygen sensing range of the sensor has a reliable limit of 1000 hPa- 1 hPa. The contactless sensor was spotted on a 250 mL Schlenk flask, where the measurement was carried out. A calibration of the instrument was done under anoxic conditions (nitrogen) and under ambient conditions (air) before starting the measurement. Furthermore, the pressure, the humidity and the temperature were necessary for the calibration. All of the measurements were carried out under atmospheric air (20.95 % O_2).

5.2.7 Quenched- phosphorescence oxygen sensing

The luminescence phase shifts were measured with a compact phase fluorometer from Pyroscience. The measurement was done in water. The excitation was performed with the light of a 624 nm LED, modulated at a frequency of 4000 Hz. The excitation-light was guided to the sensor film by an optical fibre. A RG9 emission filter (Schott) were used and the luminescence was guided back to the photodiode. Sensor foils were fixed to the end of the fibre with a screwable cop. With a cryostat (ThermoHaake DC50) the temperature was controlled to 25 °C and a gas mixing device (Voigin) was used to obtain a gas mixture of N_2 and compressed air, which was bubbled through the solution.

5.3 Synthesis

5.3.1 Reduction of quinizarine using $NaBH_4$

5.3.1.1 1,4-Anthraquinone (**1**)

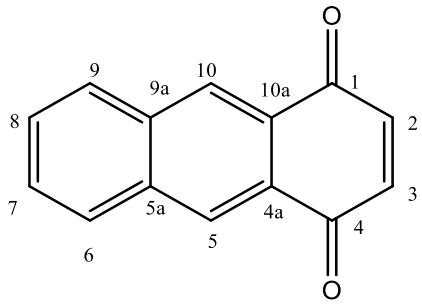

0.65 g of sodium borohydride (4.08 mmol, 5 eq.) was added in small portions to an ice-cooled (0 °C) stirred solution of 0.198 g (0.823 mmol, 1 eq.) quinizarin (1,4- dihydroxyanthraquinone) in 20 mL methanol under nitrogen atmosphere. The reaction mixture was stirred overnight. An aliquot was worked up for checking the disappearance of quinizarin by TLC (CH/EE 10:1) as described below. Before quenching the reaction solution slowly with 6M hydrochloric acid (3 mL) the reaction mixture was cooled with an ice bath. The crude product was filtered by suction, washed with distilled water and dried under reduced pressure. A silica gel column chromatography was done to purify the crude product, using CH/EE 3:1.[45]

Yield: 0.137 g, (0.57 mmol), 79.9 % o.th., orange crystals
$C_{14}H_8O_2$ [208.22]

^{1}H-NMR (300 MHz, $CDCl_3$): δ = 7.09 (s, 2H, $ArH^{2,3}$), 7.71 (m, 2H, $ArH^{7,8}$), 8.08 (m, 2H, $ArH^{6,9}$), 8.64 (s, 2H, $ArH^{5,10}$) ppm.

^{13}C-NMR (75 MHz, $CDCl_3$): δ = 128.3 (2C, $ArC^{10,5}$), 129.2 (2C, $ArC^{6,9}$), 129.8 (2C, $ArC^{7,8}$), 130.5 (2C, $C^{4a,10a}$), 135.1 (2C, $C^{5a,9a}$), 140.3 (2C, $C^{2,3}$), 185.0 (2C, $C^{1,4}$) ppm.

5.3.2 Diels-Alder cycloaddition of compound (**1**) with cyclopentadiene

5.3.2.1 1, 4, 4a, 12a-Tetrahydro-1, 4-methanonaphthacene-5, 12-dione (**2**)

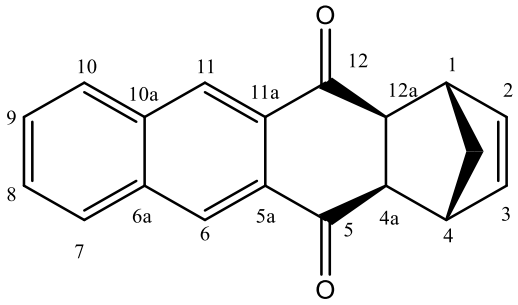

Freshly distilled cyclopentadiene (1.36 g, 20.6 mmol, 4.3 eq.) was added dropwise to a cooled solution of 1,4-anthraquinone (1.004 g, 4.82 mmol, 1 eq.) in dichloromethane (29 mL). The reaction mixture was stirred for 2 h at 0 °C and then at room temperature for 22 h. The reaction conversion was controlled by TLC (CH:EE 10:1). A full conversion could be detected. The solvent was removed under reduced pressure, and diluted with ligroin. The solid was filtered by suction, washed with ligroin and recrystallized from acetone.[48]

Yield: 1.055g, (3.85 mmol), 79.8% o.th., orange crystals
$C_{19}H_{14}O_2$ [274.3]

^{1}H-NMR (300 MHz, $CDCl_3$): δ = 1.56 (s, $ArH^{6a,10a}$); 3.52 (s, $2H^{4a,12a}$); 3.69 (s, $2H^{1,4}$); 5.96 (s, $2H^{2,3}$); 7.66-7.63 (m, $ArH^{8,9}$); 8.00-8.03 (m, $ArH^{7,10}$), 8.56 (s, $ArH^{6,11}$) ppm.

^{13}C-NMR (75 MHz, $CDCl_3$): δ = 49.60 (2C), 50.00 (2C, $C^{1,4}$), 50.11 (1C), 128.94 (2C, $C^{6,11}$), 129.44 (2C), 130.05 (2C), 131.9 (2C), 135.3 (2C, $C^{6a,10a}$), 135.8 (2C, $C^{2,3}$), 198.1 (2C, $C^{5,12}$) ppm.

5.3.3 Deprotonation and Alkylation of compound (**2**)

5.3.3.1 5,12-Dimethoxy-1,4-dihydro-1,4-methanotetracene (Monomer 1 (**3**))

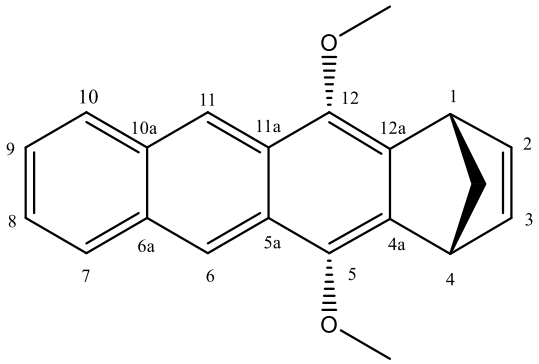

A flame-dried Schlenk flask (100 mL) was charged with NaH (0.271 g, 60 wt%, 3.1 eq). 50 mL DMF, 0.984 g compound **2** (3.59 mmol, 1.0 eq.), and 1.274 g methyl iodide (8.97 mmol, 2.5 eq.) were added under nitrogen atmosphere. The mixture was heated up to 80 °C for 3 h. There could be no full conversion detected by TLC (20:1 CH/EE) and the reaction mixture was further stirred for 1.5 h. After 1.5 hours a full conversion was detected. The reaction mixture was cooled to room temperature, diluted with distilled water (50 mL) and extracted with Et_2O (2x100 mL). The organic layers were combined, dried over Na_2SO_4, and filtered off. The solution was concentrated under reduced pressure. The crude product was purified through silica gel column chromatography using cyclohexane/ethylacetate 20:1.[1]

Yield: 0.868 g, (2.87 mmol), 78.9 % o.th., yellow crystals
$C_{21}H_{18}O_2$ [302.37]

^{1}H-NMR (300 MHz, $CDCl_3$): δ = 2.18 (d, J = 7.77 Hz, 1H, CH_2), 2.28 (d, J = 7.77 Hz, 1H, CH_2), 4.07 (s, 6H, CH_3), 4.36 (m, J = 1.70 Hz, 2H^{1,4}), 6.75 (t, J = 1.70 Hz, 2H^{2,3}), 7.44 (dd, J = 6.5, 3.2 Hz; 2ArH^{8,9}), 7.99 (dd, J = 6.4, 3.2, 2ArH^{7,10}), 8.56 (s, 2ArH^{6,11}) ppm.

^{13}C-NMR (75 MHz, $CDCl_3$): δ = 46.6, 62.2, 63.0, 120.8, 125.3, 127.3, 128.5, 131.6, 133.3, 141.1, 144.8 ppm.

5.3.4 Oligomerization of compound (**3**)

5.3.4.1 Oligomer 5,12-dimethoxy-1,4-dihydro-1,4-methanotetracene (**4a**)

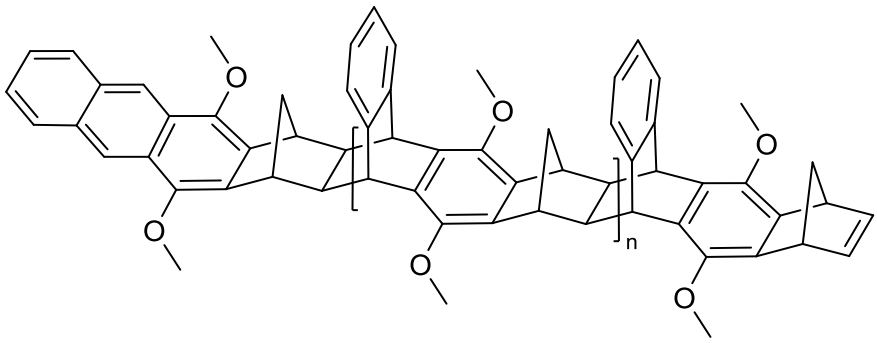

5,12-dimethoxy-1,4-dihydro-1,4-methanotetracene (**3**) was heated in the Monowave 50 to 220 °C for 18 h under nitrogen atmosphere. A small amount was sublimed and condensed on the sidewall of the vial. It was removed by using CH_2Cl_2. The dark brownish oil was used directly for the ROMP without any further purification.[1]

Yield: >99.9% o.th., brown solid

^{1}H-NMR (300 MHz, $CDCl_3$): δ = 8.57-8.49 (br, 0.4H), 8.04-7.92 (br, 0.4H), 7.48-7.36 (br, 0.4H), 7.22-6.36 (br, 3.3H), 4.86-4.44 (br, 1.5H), 4.22-3.39 (br, 6.3H), 3.32-2.97 (br, 1.2H), 2.41-1.73 (br, 2.2H), 1.42-0.74 (br, 1.1H), 0.50- -0.17 (br, 1.1H) ppm.

5.3.5 Ring opening metathesis polymerization of oligomer (**4a**) to polymer (**4b**)

5.3.5.1 Polymer 5,12-dimethoxy-1,4-dihydro-1,4-methanotetracene (**4b**)

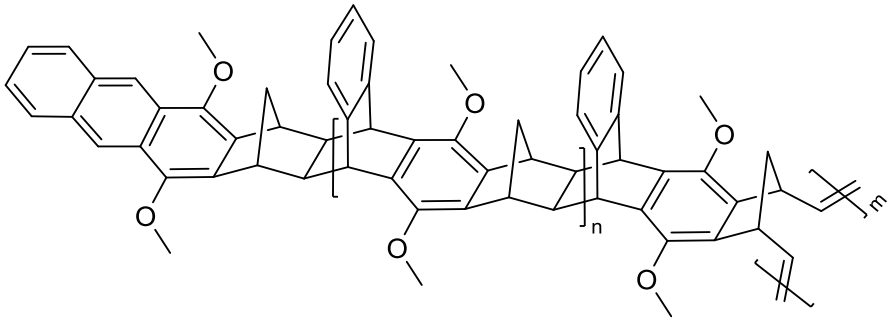

To a 25 mL Schlenk flask oligomere **4a** (71.6 mg, 0.0682 mmol, 100 eq) and 1 mL DCM were added under nitrogen amtmosphere. Subsequently, the initiator (M31) (0.51 mg, 0.000682 mmol, 1 eq.) was dissolved in 1 mL DCM and injected all at once. The reaction mixture was stirred for 12 h (48 h in case of **4b_2**) at room temperature and quenched with ethyl vinyl ether (200 µL). After another 10 minutes of stirring, the reaction mixture was precipitated in methanol and separated by centrifugation. The white solid (**4b**) was dried under reduced pressure.[1]

Yield: 34.3 mg, (0.0327 mmol), 47.9% o.th., brownish solid

^{1}H-NMR (300 MHz, $CDCl_3$): δ = 8.68-8.43 (br, 0.6H), 8.09-7.85 (br, 0.6H), 7.55-6.40 (br, 4.6H), 6.27-5.97 (br, 0.3H), 4.90-4.20 (br, 1.6H), 4.20-2.91 (br, 8.4H), 2.59-1.51 (br, 1.3H), 1.11-0.63 (br, 0.4H), 0.47- -0.31 (br, 0.4H) ppm.

5.3.6 Diels-Alder cycloaddition of anthracene and norbornadiene to compound (**5**)

5.3.6.1 (exo-1,4,4a,9,9a,10-hexahydro-9,5(1‘,2‘)-benzeno-1,4 methanoanthracene) (HBM)

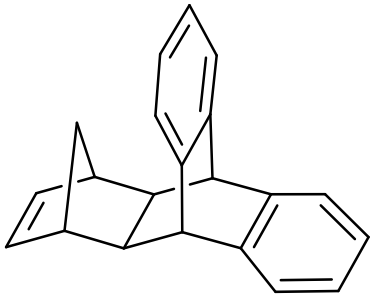

0.473 g (2.65 mmol, 1 eq.) anthracene and 1.6 mL (15.8 mmol, 6 eq.) norbornadiene were heated up to 220 °C for 2 h in the Monowave 50. The synthesis was carried out under nitrogen atmosphere. After cooling down to room temperature there was a white precipitate formed. The excess of norbornadiene was stripped from the mixture at reduced pressure. The crude product was then purified by a silica gel column chromatography using cyclohexane.[38]

Yield: 0.547 g (2.02 mmol), 76.2% o.th., white solid
$C_{21}H_{18}$ [270.38]

^{1}H-NMR (300 MHz, $CDCl_3$): δ = 7.25-6.99 (br, ArH), 6.13 (s, 2H), 4.15 (s, 2H), 2.47 (s, 2H), 2.05 (s, 2H), 0.716 (d, J = 4.58, 1H), -0.16 (d, J = 4.66, 1H) ppm.

^{13}C-NMR (75 MHz, $CDCl_3$): δ = 40.60, 43.36, 44.61, 47.73, 48.39, 48.48, 51.05, 124.1, 124.7, 125.5, 125.9, 126.1, 140.3, 142.4, 142.9, 145, 146.1 ppm.

5.3.7 Ring opening metathesis polymerization of HBM (**5**)

5.3.7.1 poly(HBM) (**5a**)

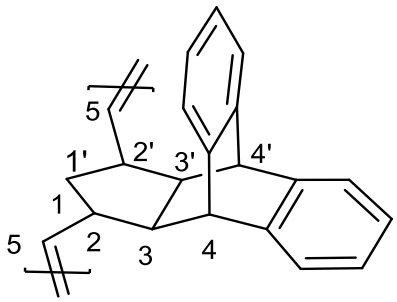

The HBM monomer (244.4 mg, 0.904 mol) was dissolved in 4 mL dichloromethane (DCM) in a 10 mL Schlenk flask equipped with a magnetic stirrer at room temperature. Under nitrogen atmosphere, an appropriate amount of the Umicore M31 ([monomer]/[M31]: 300/1), dissolved in 0.8 mL dichloromethane, was transferred into the reaction mixture and stirred for 3 h. A full conversion could be detected via TLC (CH). 200 µL of ethyl vinyl ether were added and the reaction mixture was stirred another 30 minutes at room temperature. The residue was precipitated by a drop-wise addition into vigorously stirred methanol. The polymers were stored under nitrogen atmosphere for further measurements.[65]

Yield: 0.239 mg, (0.801 mmol), 90.4% o.th., white solid

^{1}H-NMR (300 MHz, $CDCl_3$): δ = 7.61-6.35 (br, 8 ArH), 5.61-5.22 (br, 2H), 4.42-3.74 (br, 2H), 2.41-0.78 (br, 6H) ppm.

5.3.8 Hydrogenation of poly(HBM) (**5a**)

5.3.8.1 H-poly(HBM) (**6**)

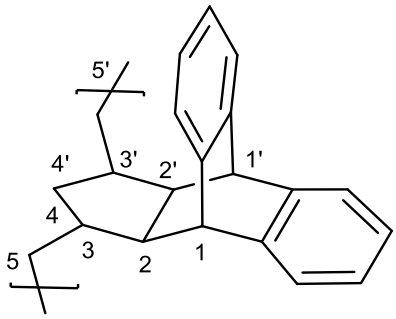

106.6 mg of poly(HBM) (**5a**) (0.394 mmol, 1 eq.), 0.367 g p-toluenesulfonyl hydrazine (1.98 mmol, 5 eq.) and 0.410 g tributylamine (2.21 mmol, 5.5 eq.) were weighed and transferred into a microwave vial under nitrogen atmosphere. 1.2 mL of toluene were added to obtain a heterogeneous mixture. The reaction was proceeded in the monowave 50 at 120 °C for 16 hours. After cooling to room temperature a clear solution was obtained. The mixture was poured into methanol to obtain a light brownish solid. After centrifugation, the polymer was washed with distilled water and redissolved in 1 mL hot toluene. The solution was again poured into methanol und centrifuged. The obtained white polymer was dried under reduced pressure.[65]

Yield: 107.5 mg, (0.355 mmol), 90.2% o.th., white solid

^{1}H-NMR (300 MHz, $CDCl_3$) δ = 7.07 (d, J=8.87), 4.14 (s, 2H$^{1,1'}$), 2.03 (s, 2H$^{2,2'}$), 1.78 (s, 1H^4), 1.54 (s, H$^{5,5'}$), 1.25 (m, H$^{5,5'}$), 0.97 (s, 2H$^{3,3'}$), 0.90 (m, H$^{4'}$) ppm.

5.3.9 Preparation of the polyHIPE

5.3.9.1 poly(NBD-co-HBM)

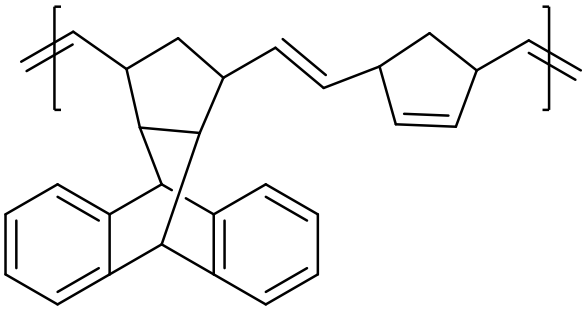

The HBM monomer (**5**) was synthesised analogous as described in the previous section *5.3.6* by using 0.47 g anthracene (2.65 mmol, 1 eq.) and 1.6 mL norbornadiene (15.7 mmol, 5.9 eq.). The HBM monomer (**5**) was directly used after the reaction in the Monowave 50 in a liquid state. According to ^{1}H-NMR spectroscopy, almost full conversion of anthracene could be obtained. A residue of 5eq (1.21 g, 15.7 mmol) unconverted norbornadiene could also be observed in the reaction mixture. The reaction mixture and 0.134 g of the surfactant Span 80 were mixed and stirred. Furthermore, 0.37 mg (40000:1) of the catalyst Grubbs M2 was dissolved in 100 µL toluene and added to the reaction mixture. To obtain a porosity of 80 %, 7.68 mL water were added dropwise and the reaction mixture was stirred for 1 h. After curring at 40 °C for 2 h in a drying cabinet, the polyHIPE was washed with acetone and further stored under nitrogen atmosphere.

5.3.10 Preparation of the sensor films

The sensor foils for the quenched- phosphorescence oxygen sensing were prepared by knife coating cocktails of comparable viscosity onto a Mylar® support from Goodfellow (poly(ethylene glycol terephthalate)) by using a 2.5 µm spaced Gardener coating knife.
For the preparation of the cocktails, 1.35 mg of the $PtTPTBPF_4$ were dissolved in 1 mL chloroform to yield a concentration of 1.35 g/L. The cocktails typically contain 10 wt% of polymer in chloroform and 1 wt% of $PtTPTBPF_4$. Some additional chloroform was added to achieve a lower viscosity. The weighted amounts for the three prepared cocktails are shown in Table 9. After casting, the sensor foils were dried overnight at 60 °C for the complete removal of the solvent.[62]

Table 9: Preparation of the sensor foils

	Polymer (4b) foil	**Poly(HBM) (5a) foil**	**Poly(H-HBM) (6) foil**
Polymer	20 mg	19.6 mg	20.7 mg
$CHCl_3$	62.4 µL	54.8 µL	57.1 µL
$PtTPTBPF_4$ in $CHCl_3$ c= (1.35 g/L)	118 µL	116 µL	112 µL

6. List of Abbrevations

Analytical Methods

ATR-IR	Attenuated Total Reflection Infrared Spectroscopy
Hz	Hertz
MHz	Megahertz
NMR	Nuclear Magnetic Resonance
J	Coupling constant
s	Singlet
d	Doublet
t	Triplet
q	Quadruplet
m	Multiplet
ppm	Part per million
BET	Brunauer-Emmett-Teller model
DSC	Differential Scanning Calorimetry
GPC	Gel Permeation Chromatography
TLC	Thin Layer Chromatography

Chemical formula

$CDCl_3$	Deuterated chloroform
NaOH	Sodium hydroxide
EE	Ethylacetate
CH	Cyclohexane
DCM	Dichloromethane
NaCl	Sodium chloride
MeOH	Methanol
$CHCl_3$	Chloroform
DMF	Dimethylformamide
Cp	Cyclopentadiene
NBD	Norbornadiene

PS	Polystyrene

Others

μ	Mikro
τ	Lambda
ρ	Density
wt%	Weight percent
UV	Ultraviolet
ROMP	Ring opening metathesis polymerization
PolyHIPE	Polymerised high internal phase emulsion
POP	Porous Organic Polymers
MOF	Metal organic framework
COF	Covalent organic framework

7. List of Figures

8. List of Tables

9. List of Equations

10. Literature

1. Zhao, Y., He, Y. & Swager, T. M. Porous Organic Polymers via Ring Opening Metathesis Polymerization. *ACS Macro Lett.* **7,** 300–304 (2018).
2. Borisov, S. M. Fundamentals of Quenched and Rational Design of Sensor Materials. 1–18
3. Wood, C. D. *et al.* Microporous organic polymers for methane storage. *Adv. Mater.* (2008).
4. Kaur, P., Hupp, J. T. & Nguyen, S. T. Porous Organic Polymers in Catalysis : Opportunities and Challenges. *Perspective* 819–835 (2011).
5. Bracco, S. *et al.* Porous 3D polymers for high pressure methane storage and carbon dioxide capture. *J. Mater. Chem. A* (2017).
6. Jiang, J. X. *et al.* Microporous poly(tri(4-ethynylphenyl)amine) networks: synthesis, properties, and atomistic simulation. *Macromolecules* (2009).
7. El-Kaderi, H. M. *et al.* Designed Synthesis of 3D Covalent Organic Frameworks. *Science* **316,** 268–272 (2007).
8. Ben, T. *et al.* Targeted synthesis of a porous aromatic framework with high stability and exceptionally high surface area. *Angew. Chemie - Int. Ed.* (2009).
9. Wu, D. *et al.* Design and preparation of porous polymers. *Chemical Reviews* **112,** 3959–4015 (2012).
10. Dawson, R., Cooper, A. I. & Adams, D. J. Chemical functionalization strategies for carbon dioxide capture in microporous organic polymers. *Polymer International* (2013).
11. Gokmen, M. T. & Du Prez, F. E. Porous polymer particles - A comprehensive guide to synthesis, characterization, functionalization and applications. *Progress in Polymer Science (Oxford)* (2012).
12. Dawson, R. and A. T. *Porous Polymers: Design, Synthesis and Applications. Chapter 7: Conjugated microporous polymers*. *Royal Society of Chemistry. Monographs in Supramolecular Chemistry No. 17* (2015).
13. Huo, Q. Synthetic Chemistry of the Inorganic Ordered Porous Materials. in *Modern Inorganic Synthetic Chemistry* (2011).
14. Silverstein, M. S., Cameron, N. R. & Hillmyer, M. *Porous Polymers*. *Porous Polymers* (2011).
15. Bildirir, H., Gregoriou, V. G., Avgeropoulos, A., Scherf, U. & Chochos, C. L. Porous organic polymers as emerging new materials for organic photovoltaic applications: Current status and future challenges. *Materials Horizons* **4,** 546–556 (2017).

16. Sing, K. S. W. *et al.* REPORTING PHYSISORPTION DATA FOR GAS / SOLID SYSTEMS with Special Reference to the Determination of Surface Area and Porosity (Recommendations 1984). *Pure Appl. Chem.* (1985).
17. Gao, H. & Matyjaszewski, K. Synthesis of functional polymers with controlled architecture by CRP of monomers in the presence of cross-linkers: From stars to gels. *Progress in Polymer Science (Oxford)* (2009).
18. Matyjaszewski, K. Architecturally complex polymers with controlled heterogeneity. *Science* (2011).
19. Ahmed, D. S., El-Hiti, G. A., Yousif, E., Ali, A. A. & Hameed, A. S. Design and synthesis of porous polymeric materials and their applications in gas capture and storage: a review. *J. Polym. Res.* (2018).
20. Zhou, H. C., Long, J. R. & Yaghi, O. M. Introduction to metal-organic frameworks. *Chemical Reviews* (2012).
21. Tranchemontagne, D. J., Mendoza-Cortés, J. L., O'Keeffe, M. & Yaghi, O. M. Secondary building units, nets and bonding in the chemistry of metal-organic frameworks. *Chem. Soc. Rev.* (2009).
22. Furukawa, H., Cordova, K. E., O'Keeffe, M. & Yaghi, O. M. The chemistry and applications of metal-organic frameworks. *Science* (2013).
23. Li, Q. & Thonhauser, T. A theoretical study of the hydrogen-storage potential of (H2)4CH4 in metal organic framework materials and carbon nanotubes. *J. Phys. Condens. Matter* (2012).
24. Ding, S.-Y. & Wang, W. Covalent organic frameworks (COFs): from design to applications. *Chem. Soc. Rev.* (2013).
25. Wu, M. X. & Yang, Y. W. Applications of covalent organic frameworks (COFs): From gas storage and separation to drug delivery. *Chinese Chemical Letters* (2017).
26. Cote, A. P. *et al.* Porous , Crystalline , Covalent Organic Frameworks. *Science (80-.).* **130,** 1166–1171 (2008).
27. Cote, A. P. Porous, Crystalline, Covalent Organic Frameworks. *Science (80-.).* (2005).
28. Holst, J. R., Stöckel, E., Adams, D. J. & Cooper, A. I. High surface area networks from tetrahedral monomers: Metal-catalyzed coupling, thermal polymerization, and 'click' chemistry. *Macromolecules* **43,** 8531–8538 (2010).
29. Calderon, N. The Olefin Metathesis Reaction. *Acc. Chem. Res.* **5,** 127–132 (1972).
30. Movassaghi, M. The olefin metathesis reaction. *J. Am. Chem. Soc* **119,** 3887–3897 (1997).
31. Bielawski, C. W. & Grubbs, R. H. Living ring-opening metathesis polymerization. *Prog.*

Polym. Sci. **32,** 1–29 (2007).

32. Nguyen, S. T., Johnson, L. K., Grubbs, R. H. & Ziller, J. W. Ring-Opening Metathesis Polymerization (ROMP) of Norbornene by a Group-VIII Carbene Complex in Protic Media. *J. Am. Chem. Soc.* **114,** 3974–3975 (1992).
33. Quigley, B. L. & Grubbs, R. H. Ruthenium-catalysed Z-selective cross metathesis of allylic-substituted olefins. *Chem. Sci.* **5,** 501–506 (2014).
34. Scholl, M., Ding, S., Lee, C. W. & Grubbs, R. H. Synthesis and activity of a new generation of ruthenium-based olefin metathesis catalysts coordinated with 1,3-dimesityl-4,5-dihydroimidazol- 2-ylidene ligands. *Org Lett* **1,** 953–956 (1999).
35. Choi, T.-L. & Grubbs, R. H. Controlled-living polymerization by fast-initiating ruthenium catalyst. in *Abstracts of Papers, 225th ACS National Meeting, New Orleans, LA, United States, March 23-27, 2003* POLY-014 (2003).
36. Shin, J. Y., Park, J. Y., Liu, C., He, J. & Kim, S. C. Chemical structure and physical properties of cyclic olefin copolymers (IUPAC Technical Report). *Pure Appl. Chem.* **77,** (2005).
37. Cui, J., Yang, J.-X., Pan, L. & Li, Y.-S. Synthesis of Novel Cyclic Olefin Polymer with High Glass Transition Temperature via Ring-Opening Metathesis Polymerization. *Macromol. Chem. Phys.* **217,** (2016).
38. Hong, M., Cui, L., Liu, S. & Li, Y. Synthesis of novel cyclic olefin copolymer (COC) with high performance via effective copolymerization of ethylene with bulky cyclic olefin. *Macromolecules* **45,** 5397–5402 (2012).
39. Mao, D. *et al.* Preparation of macroporous polyHIPE foams via radiation-induced polymerization at room temperature. *Colloid Polym. Sci.* (2013).
40. Cameron, N. R. High internal phase emulsion templating as a route to well-defined porous polymers. *Polymer* (2005).
41. Barbara, I., Dourges, M. A. & Deleuze, H. Preparation of porous polyurethanes by emulsion-templated step growth polymerization. *Polym. (United Kingdom)* **132,** 243–251 (2017).
42. Naranda, J. *et al.* Polyester type polyHIPE scaffolds with an interconnected porous structure for cartilage regeneration. *Sci. Rep.* **6,** (2016).
43. Zapp, K.-H. Anthraquinone Dyes and Intermediates. *Ullmann's Encycl. Ind. Chem.* (2012).
44. Barbosa, J., Sanchez, J. & Bosch, E. Study of 1,4-dihydroxyanthraquinone as an acid-base indicator in isopropyl alcohol medium. Evaluation of colour-change limits through complementary chromaticity parameters. *Talanta* (1984).
45. Nor, S. *et al.* Synthesis of New Cytotoxic Aminoanthraquinone Derivatives via

Nucleophilic Substitution Reactions. *Molecules* (2013).

46. Vollhardt, P. & Schore, N. Organic Chemistry: Structure and Function. in *W.H.Freeman and Company* (2015).
47. Houk, K. N. & Luskus, L. J. The Influence of Steric Interactions on Endo Stereoselectivity. *J. Am. Chem. Soc.* (1971).
48. Patney, H. K. & Paddon-Row, M. N. An Improved Synthesis of 2,3-Norbornadienoanthracene and its Application to the Synthesis of Anthracene Annellated Norbornenylogs. *Synthesis (Stuttg).* (1986).
49. Paquette, L. e-EROS Encyclopedia of Reagents for Organic Synthesis. in *Encyclopedia of Reagents for Organic Synthesis V.4* (2009).
50. Wiberg, N., Holleman, A. F. & Wiberg, E. *Holleman-Wiberg's Inorganic Chemistry*. *Journal of Chemical Education* (2002).
51. Cox, E. G. Structural inorganic chemistry. *Nature* (1951).
52. Long, T. E. & Hunt, M. O. Solvent-Free Polymerizations and Processes : Recent Trends in the Minimization of Conventional Organic Solvents. 1–5 (1999).
53. Skoog, D. A., Holler, F. J. & Crouch, S. R. *Principles of Instrumental Analysis Sixth Edition*. *Thompson Brooks/Cole* (1998).
54. Moore, J. C. Gel permeation chromatography. I. A new method for molecular weight distribution of high polymers. *J. Polym. Sci. Part A Gen. Pap.* (1964).
55. Brunauer, S., Emmett, P. H. & Teller, E. Adsorption of Gases in Multimolecular Layers. *J. Am. Chem. Soc.* (1938).
56. Sing, K. S. W. Adsorption methods for the characterization of porous materials. *Adv. Colloid Interface Sci.* (1998).
57. Handbook of Thermal Analysis and Calorimetry. *Handb. Therm. Anal. Calorim.* (2008).
58. Cui, J., Yang, J. X., Li, Y. G. & Li, Y. S. Synthesis of high performance cyclic olefin polymers (COPs) with ester group via ring-opening metathesis polymerization. *Polymers (Basel).* (2015).
59. Wolfbeis, O. S. Materials for fluorescence-based optical chemical sensors. *Journal of Materials Chemistry* (2005).
60. Schweitzer, C. & Schmidt, R. Physical Mechanisms of Generation and Deactivation of Singlet Oxygen. *Chem. Rev.* **103,** 1685–1758 (2003).
61. Wang, X. D. & Wolfbeis, O. S. Optical methods for sensing and imaging oxygen: Materials, spectroscopies and applications. *Chemical Society Reviews* (2014).
62. Koren, K. *et al.* Tuning the dynamic range and sensitivity of optical oxygen-sensors by employing differently substituted polystyrene-derivatives. *Sensors Actuators, B Chem.*

(2013).
63. Wolfbeis, O. S. Fiber-optic chemical sensors and biosensors. *Analytical Chemistry* (2008).
64. Ghauharali, R. I. & Brakenhoff, G. J. Fluorescence photobleaching-based image standardization for fluorescence microscopy. *J. Microsc.* (2000).
65. Yang, J. X., Cui, J., Long, Y. Y., Li, Y. G. & Li, Y. S. Synthesis of cyclic olefin polymers with high glass transition temperature by ring-opening metathesis copolymerization and subsequent hydrogenation. *J. Polym. Sci. Part A Polym. Chem.* (2014).